

# Effects of hydroxyapatite addition on the microstructure and mechanical properties of sintered magnesium matrix composites

S. Jayasathyakawin<sup>1</sup>, M. Ravichandran<sup>1,\*</sup>, Sikiru Oluwarotimi Ismail<sup>2</sup>, D.Srinivasan<sup>1</sup>

<sup>1</sup>Department of Mechanical Engineering, K. Ramakrishnan College of Engineering, Samayapuram, Trichy – 621112, Tamil Nadu, India

<sup>2</sup>Department of Engineering, Centre for Engineering Research, School of Physics, Engineering and Computer Science, University of Hertfordshire, AL10 9AB, Hatfield, UK

\*Corresponding Author: E-mail:smravichandran@hotmail.com, Tel.: +918248165224

## Abstract

This study focused on the microstructure and properties of magnesium alloy (Mg/3Al)-based composites, reinforced with hydroxyapatite (HA) and produced by powder metallurgy (PM) method. In this investigation, Mg alloys were reinforced on the basis of weight percentage (wt.%) of HA to produce Mg3Al alloy as well as Mg3Al/3HA, Mg3Al/6HA and Mg3Al/9HA composite samples. Measurements were taken based on their properties, including density, hardness, compressive strength, wear rate (WR) and corrosion behaviour. Microstructural studies on the various Mg3Al/HA composites were carried out, using scanning electron microscopy (SEM), energy dispersive X-ray spectroscopy (EDS) and X-ray diffraction (XRD). Wear behaviours of the composites were analysed with aid of Taguchi method. Worn surface analysis was performed, using SEM. From the results obtained, better wear resistance property was obtained with the sample Mg3Al/9HA. Evidently, the addition of HA content to the Mg/3Al alloy increased its mechanical strength, due to uniform distribution of HA in the matrix. From signal-to-noise (S/N) ratio analysis, it was observed that the optimum parameters were obtained at HA content of 9 wt.%, speed of 2 m/s, displacement of 750 m and applied load of 5 N for minimum WR. Similarly, the optimal parameters for minimal coefficient of friction (COF) were 9 wt.%, 1 m/s, 750 m and 5 N. Leveraging from these composite samples, the results obtained stand to advance knowledge on tribology of composite materials, guide the choice and application of the materials, especially where wear and friction are inevitable.

**Keywords:** Composite; Magnesium alloy; Hydroxyapatite; Corrosion; Properties; Powder metallurgy.

## 1. Introduction

Magnesium (Mg) is a lightest alternative metallic material for aluminium (Al) related composites, which are widely required in different parts of equipment used in aerospace and many industrial sectors [1-3]. The major advantage of the Mg-based metal includes medical applications [4]. The density of Mg is 67, 25 and 20% of Al, zinc (Zn) and steel, respectively. Mg composites are well known to orthopaedics [5]. In the automobile industry, Mg composite reduces the structural weight, increases fuel efficiency and improves the mechanical property [6]. Mg matrix composites are largely used to increase the strength of materials for medical applications through an easy scientific method for elastic property [7,8]. In biomedical applications, Mg-based bio-composites are used for dental implants, bone screws, bone fixation and cardiovascular stents. Mg is a key material in the engineering field. Mg has better stiffness, huge damping capacity, good bonding features, less density, higher strength, biodegradability, biocompatibility, bioactivity and it is a biomaterial, considering environments [9,10]. The main objective of the biomedical field is to control corrosion and advance increase in mechanical strength of the human bone, which is achieved using Mg. Many literature surveys have focused on the ductility and strength of pure Mg with an increasing diversity of reinforcements [11,12]. Singh et al. [13] concluded that the degradable biomaterials, such as Mg alloys recently became the focus of worldwide orthopedic device research. After complete healing of the tissues, the implant is shielded from severe stress to reduce the need for a second surgery for implant removal.

Hydroxyapatite (HA) plays a vital role in organic coating for load-carrying bio implant and bone screws. Recently, HA-based coatings on the Mg composite have attracted many orthopaedic applications. The performance of Mg and titanium dioxide (TiO<sub>2</sub>) reinforced in HA has improved the surface structure, microstructure characterisation, mechanical property, interfacial bonding toughness, wear-resistance, hardness value and corrosion activity. Similarly, Mg and HA increased the cohesive strength, microhardness value, bio related activity and anti-wear corrosion of coatings [4,14]. Calcium phosphates (CaP) is a vital substance for HA to increase bone tissue healing. The application of the HA include pharmaceutical products, water therapy and protein chromatography. HA could help the bone healing process. Orthopaedic applications of HA has osteoinductive and osteoconductive performances in the human body. Mg composite with nano-HA can be developed by many surface coating processes, such as sol-gel processing, electrochemical deposition and spray

coating for biomedical application. Production of nano HA coating on Mg-based composites is an easy process and low cost [10]. HA helps the bone healing process and bone growing process in the human body naturally. Nanopowder of HA and Mg-based composite attain good biomineralisation to the body and it has twice the workability of conjoining representative and human production reinforcement. The nano-HA powder improved the mechanical property of biocomposite, such as grain size, specific surface and composition in biomaterials [2,15]. HA is predominantly selected as a reinforcement for Mg composite [3]. In biomedical applications, reinforcements of HA and  $\beta$ -tricalcium phosphate are suitable materials for the human body. They are produced by powder metallurgy (PM) technique [16,17].

Moving forward, PM has many advantages toward production of composite with easy methods. The production temperature is low and reinforcement distribution is constant [18]. In PM process, sintering is the most important process to obtain good microstructure characterisation, high density and bonding between the particles [4,19]. The PM technique is used to produce Mg matrix composites. When compared with ingot metallurgy and PM process, the PM technique increased the growth of smaller grain structures and superplastic performance in elevated strain rate [20-22]. HA with AZ91D matrix improved the corrosion property, because it contained a cytocompatible organic material [23]. In comparison with casting, PM method resulted to a better microstructural development and greater refinement of grain structure [24]. Considering biomedical applications, PM process is an effective method of fabricating composite materials for human body bio-implant with very safe conditions in the biological environment [25-28].

Topuz et al. [29] investigated into the titanium matrix composite reinforced with HA and  $ZrO_2$  and fabricated by using PM technique. It was reported that PM route was also suitable for the production of titanium matrix composite and HA+ $ZrO_2$  improved the microstructure, mechanical and corrosion properties of the bulk and scaffold of Ti/HA+ $ZrO_2$  composites. Xie et al. [30] produced Ti-10wt.%Mo matrix biocomposite reinforced with HA, using PM process. It was reported that addition of HA improved the corrosion resistance of the composites and the ceramic phases, and micropores in Ti-10wt.%Mo/HA composites increased the bioactivity applications. Ghazizadeh et al. [31] examined the Mg matrix composite reinforced with HA and manufactured by using mechanical-electromagnetic stirring method. Two composites were studied: Mg-2.5wt.%HA and Mg-5wt.%HA before

summarised that both tensile and compressive strengths of Mg-5wt.%HA composite improved.

In a recent study, Singh et al. [14] developed a method for applying HA reinforced with TiO<sub>2</sub> to an alloy of titanium-35Nb-7Ta-5Zr, using plasma spray deposition technique. Analyses of the effects of TiO<sub>2</sub> reinforcement on coating properties, microstructure, corrosion resistance and in-vitro bioactivity were conducted. Jaiswal et al. [2] explained that several biocompatible materials can be added to Mg-based composites, including bio glass, inert alumina and HA, which shared both its chemical composition and crystal structure with bone. Cui et al. [3] investigated into the dispersion of HA particles in the AZ91D/HA composite, developed by the PM method. It was concluded that the corrosion rate and mechanical properties of the composites were significantly impacted by the dispersion of HA particles. Akmal et al. [32] reported that bioactive metals, such as HA can be reinforced with nickel titanium (NiTi)-based bioimplant to produce good mechanical performance, biocompatibility and bioactivity. Prakash et al. [33] examined that Mg-Nb-HA composite could be manufactured by microwave sintering process for orthopaedic application and summarised that it has less elastic modulus and better corrosion resistance. Zhao et al. [34] explained that substances, such as HA whisker, zirconium and bioglass can be used as reinforcements to synthesise HA-based biocomposites. Other studies on Mg-based biomaterial samples, which were manufactured by PM technique have been reported [35-37]. Bansal et al. [38] reported that mineral zinc was one of the most prevalent constituents of hard tissues. As a protective agent and component in the Mg alloy AZ31, it played an important role in cellular growth. Additionally, it supported many physiological functions related to the immune system.

Roshan et al. [39] studied AZ31 surface alloy coated with hybrid chitosan-HA for anti-corrosion and *in-vitro* anti-corrosion protection in an environment. It was reported that corrosion resistance improved with the coated samples, which were studied by using potentiodynamic polarisation and electrochemical impedance spectroscopy tests. Singh et al. [40] investigated into the ZM21 Mg alloy coated with PCL/HA/TiO<sub>2</sub> and concluded that the coating improved the corrosion behaviour, biocompatibility and mechanical properties.

Furthermore, Guan et al. [41] studied both solution and aging strengthening, as zinc helped to strengthen the matrix. These improvements contributed to corrosion resistance and electrical potential. Selvam et al. [42] observed dry sliding wear on Mg matrix composites made by PM, zinc oxide nanoparticle reinforcement was used. Garcia-Rodrigueza et al. [43]

conducted an analysis of dendritic Mg alloys and composites for sliding wear, it was concluded that AZ91 cast Mg alloy showed a two-phase wear behaviour characterised by mild and severe wears, respectively. Severe wear was characterised by melt wear and mild wear by oxidative delamination wear. Taltavull et al. [44] studied the dry sliding pin-on-disc test, the wear resistance of the AM60B Mg alloy was examined, using laser surface melting (LSM). Lopez et al. [45] investigated into the wear behaviour of an extruded Mg alloy of grade ZE41A with T5 heat-treatment condition by using a pin-on-disc wear apparatus against grade F112 steel. Different wear regimes were observed in the tested material, depending on the load and sliding velocity. Yong et al. [46] concluded that the composite of Mg<sub>2</sub>Si/AM60 or Mg matrix composites recorded increased wear resistance properties with an increasing silicon (Si) content, and decreased wear properties with increasing applied load and sliding rate. Mg matrix composite made of Mg<sub>2</sub>Si/AM60 exhibited an abrasive wear mechanism that transformed into adhesion wear, as the load was increased. Bolin et al. [47] studied the treated and untreated samples of the Mg alloy AZ91D, tested experimentally for wear resistance. Comparing the treated and untreated samples of the AZ91D alloys, the treated surface layer displayed enhanced wear resistance. AZ91D possessed a better wear resistance and a longer impact time produced a higher impact current. Khalajabadi et al. [48] developed Mg-HA-TiO<sub>2</sub>nanocomposite, using milling-pressing-sintering technique. It was concluded that Mg-HA-TiO<sub>2</sub>nanocomposite improved corrosion resistance and mechanical properties of the biodegradable implants.

Based on the aforementioned extensive literature, several manufacturing processes have been used to support the relevance of HA and other particles as reinforcements in Mg-based composites. However, there is no reported study exactly on influences of HA addition on both microstructure and mechanical properties of sintered Mg matrix composites, specifically with variable HA filler contents (wt.%) and using PM technique. Therefore, the present work studied various Mg<sub>3</sub>Al/HA composite samples, which were manufactured through PM technique. The microstructure, mechanical and corrosion properties of the proposed composites were analysed. The worn surfaces of the samples were thoroughly studied, using scanning electron microscopy (SEM). The suitable wear parameters were identified, based on signal-to-noise (S/N) ratio analysis. The contour and probability plots were provided for better understanding of the influence of wear parameters on the wear rate (WR) and coefficient of friction (COF). The optimal process parameters were obtained for the best composite sample.

## 2. Experimental procedure

Samples of Mg3Al as well as Mg3Al/3HA, Mg3Al/6HA and Mg3Al/9HA were produced, using powders of Mg, Al and HA. Pure Mg and Al from Kemphasol Co. Ltd, Mumbai, India; purity: 99% (K08019), particle size: <200µm and nano HA from Nano Research Laboratory Company, Jharkhand, India; purity: 99.5%, APS 30-50 nm and molecular formula: Ca<sub>5</sub>(OH)(PO<sub>4</sub>)<sub>3</sub> powders were used as raw materials. Fig. 1 shows the proposed work plan for the investigation.

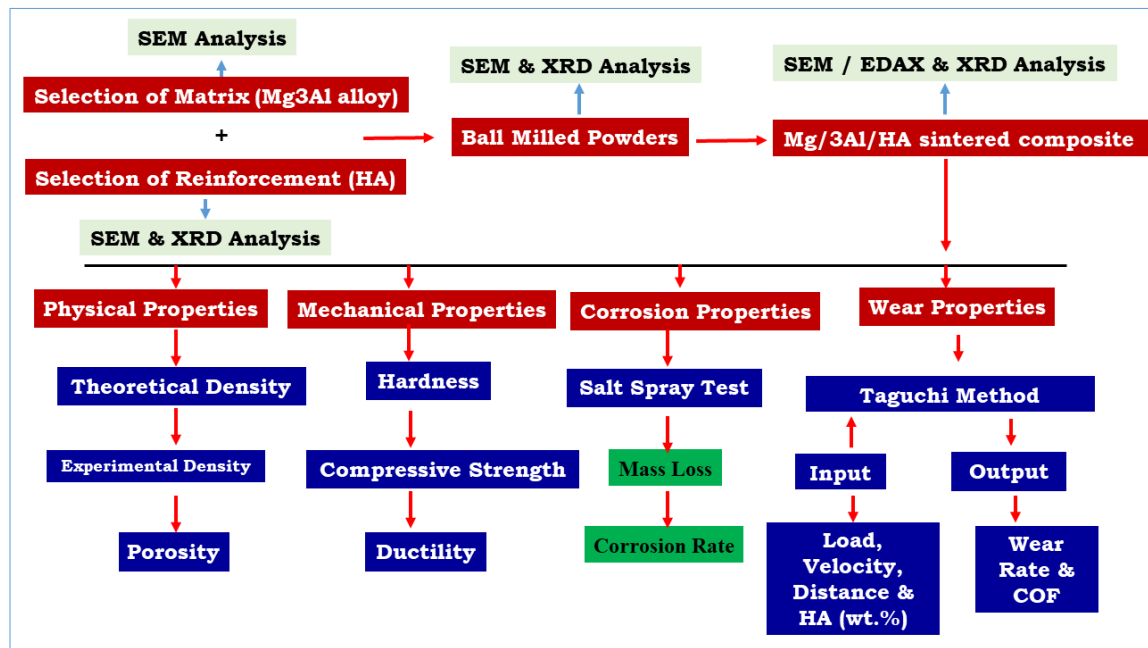
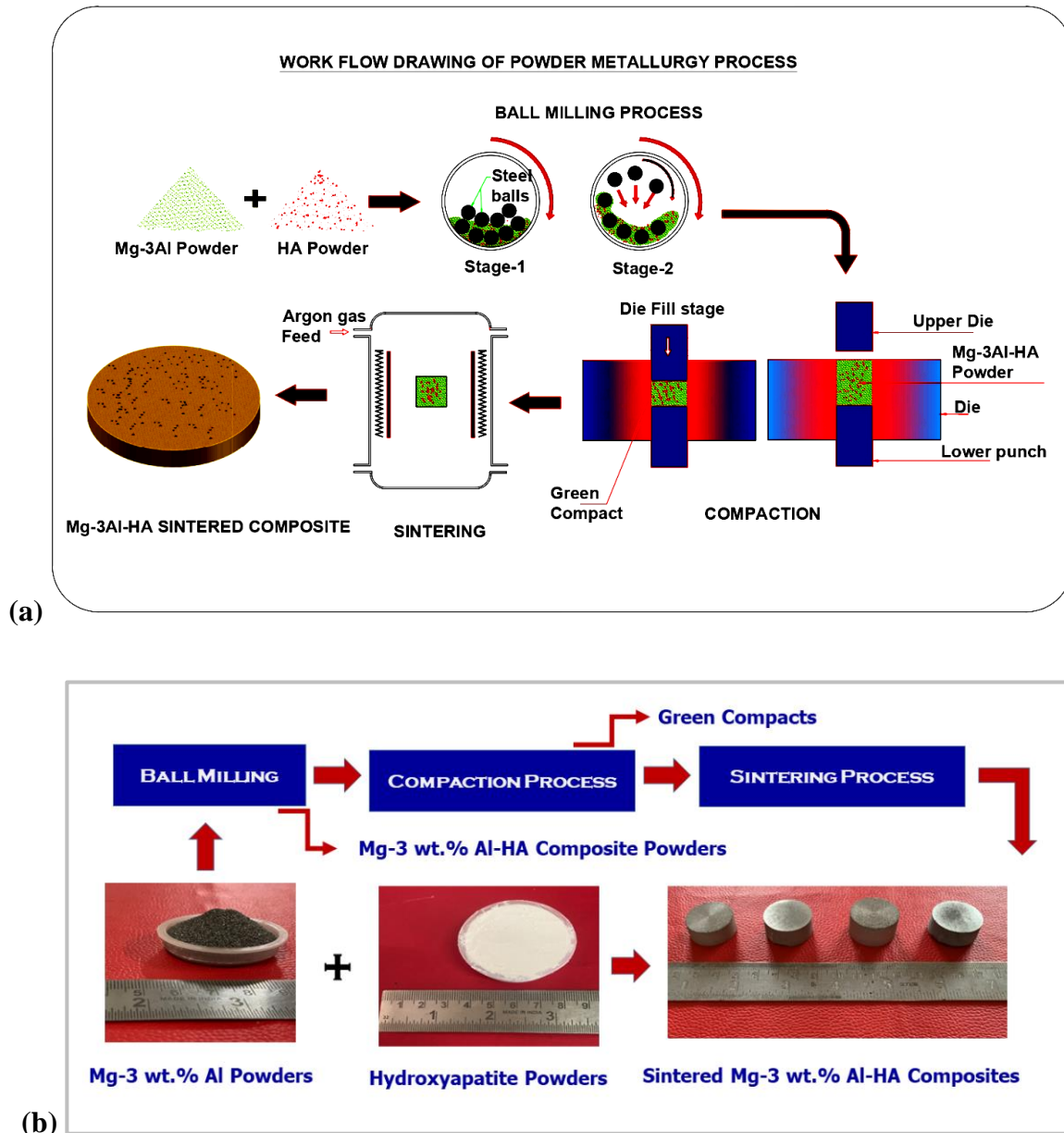


Fig. 1 Proposed work plan.

In this work, 3 wt.% of Al was added to the Mg to improve the strength and ductility of the Mg. Al is a popular alloying element for Mg to form the Mg-Al binary alloys. From the same review article, Al is classified as an allergic element, not toxic [56]. The microstructure, mechanical and corrosion properties of the proposed composites were only and mainly analysed in this present study. However, this study will be advanced to include both *in-vitro* and *in-vivo* tests in order to investigate into their biocompatibility for biomedical applications, as the work progresses. From the same review article, Al is classified as an allergic element, not toxic [56]. The microstructure, mechanical and corrosion properties of the proposed composites were only and mainly analysed in our manuscript. However, we can advance the study with *in-vitro* and *in-vivo* tests to investigate into their biocompatibility for biomedical applications, as the work progresses. Figs 2(a) and (b) show the schematic

diagram for the fabrication of the various Mg3Al/HA composites and the photographic images of Mg powders, HA powders and sintered composite samples, respectively.



**Fig.2(a)** Schematic diagram of the fabrication process of Mg3Al/HA composites and **(b)** photographic images of Mg powders, HA powders and sintered composite samples.

The mixture (Mg/Al) of matrix material and reinforcing powder (HA) was chosen, and denoted as Mg+Al+HA. The Mg+Al+nano HA mixtures in varying proportions of 0, 3, 6 and 9 wt.% were milled by high-speed ball milling, using tungsten carbide balls for 120 rpm and 180 minutes for each sample. Then, it was uniaxially pressed at 400-500 MPa until the

powder was compacted to the dimensions of 12\*24 mm. Compaction was achieved with the help of digital hydraulic press (Model: Venus Tun-400).

Moreover, argon controlled furnace (Model: Hi Tech 1200°C) was used to heat the mixture; Mg+Al+HA materials at a temperature that provided a protective atmosphere during sintering. The process was performed at 450°C without soaking and in a protective atmosphere for two hours with the heating rate of 10°/minutes. The density of the sample was determined based on the Archimedes' principle, using a density measurement kit. By applying the rule of mixture, the theoretical density and percentage porosity were calculated. For a track record, a weighing balance machine was used to obtain the weight of each sample. Using the rule of mixtures, the theoretical densities of the as-prepared Mg, Al and HA composites were calculated. Mg, Al and HA have densities of 1.74, 2.70, 3.16 g/cm<sup>3</sup>, respectively. After mechanical polishing, the actual densities of Mg3Al/HA composites and Mg3Al samples were analysed by Archimedes' principle, using a density tester.

The microstructure examination was performed, using SEM (Make: TESCAN VEGA3-Wsource). Standard mechanical polishing techniques were employed to prepare the samples and then they were etched for 10 and 12 seconds to observe the microstructure. Figs 3(a) and (b) depict the SEM images of Mg and HA powders, respectively.

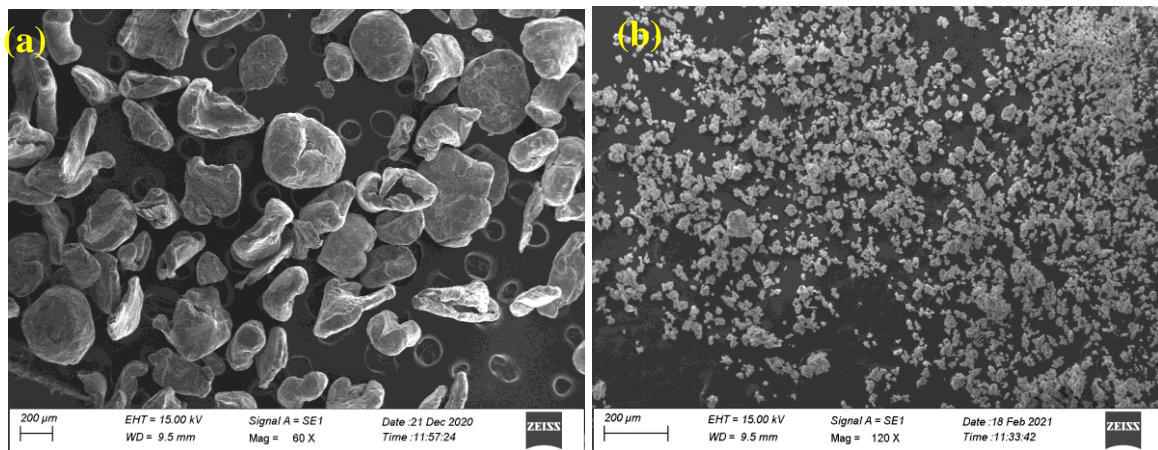


**Fig.3.** SEM images of as-received (a) Mg and (b) HA powders.

Fig. 4 shows the X-ray diffraction (XRD) pattern of as-received HA powder and its required plane. For phase identification, an XRD experiment was carried out, using Malvern Panalytical X Pert<sup>3</sup> Powder System with a CuK $\alpha$  ( $\lambda = 1.54060\text{\AA}$ ) radiation source and an image-plate detector over 5 to 89° range for the fabricated samples.

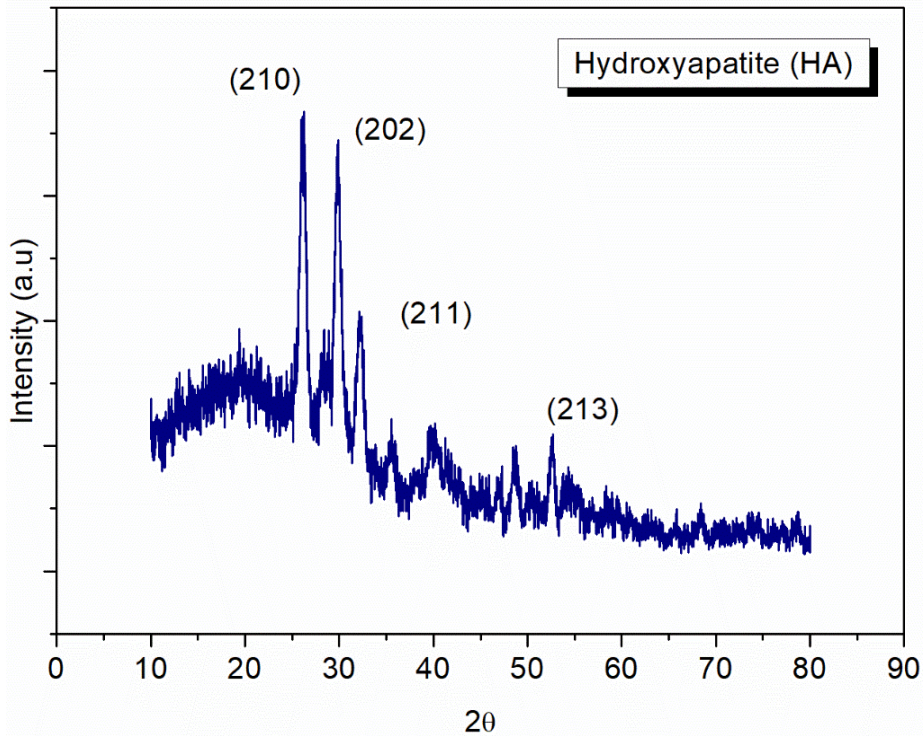


**Fig. 4.** XRD pattern of as-received HA powder.

In accordance with ASTM standard E384-99, an automatic digital micro-hardness tester (Model: Holmarc MV1-PC) was operated with a load of 1 kg and a dwell time of 15 seconds on the Mg3Al alloys and HA milled Mg composite samples. Computer control universal testing machine (CCUTM) (Model: M50) with a crosshead speed of 3mm/min was used to conduct the compression test on the Mg and Mg/HA composite surfaces, according to the ASTM E-9 standards. Generally, the metal matrix composites produced via PM route has porosity defect issues [57]. From many studies/literatures, it is understood that, both the compressive and tensile strengths of the composite samples increased with for the increase in the weight or volume percentage of the reinforcement particles [58-61]. However, the strength of the composites was lower for the samples fabricated through PM than other liquid based methods, such as casting, ~~in-situ etc.~~ [62]. This shows the limitation of the PM process. However, the strength of the composites could be improved after secondary processing including ~~such as~~ extrusion, hot forging and ~~and~~ cold forging, among others ~~etc~~ [63-65]. Each sample was tested by salt spray, using ASTM B-117. For passive diffusion tests, samples were placed in an enclosed chamber and sprayed continuously with a 5 wt.% of NaCl solution. Adding buffer solution, the pH value of the solution was maintained at 7.5. Air was atomised continuously within pressure of 2 to 3 bars by regulating the pressure. During the test, the temperature ranged from 33 to 35 °C. A pH measurement was taken once every eight hours. A hygrometer was used to measure humidity, which reached 98% during the test. The salt spray corrosion test was used to analyse the corrosion behaviour of the proposed composite samples. Even though the proposed materials ~~may would~~ be suitable for biomedical application, initially ~~this we study focused on~~ the corrosion behaviour in NaCl solution. The corrosion study using body fluid ~~will will~~ be reported in our future publications.

Besides, a pin-on-disc (Make:Ducom Wear test) experimental setup was used to calculate wear and frictional force. Two samples were needed for the pin-on-disc wear test to be conducted. During the pin-on-disc test, the pin entered the circular counter plate at a perpendicular angle. With a disc rotating at a specific speed and a pin sample being pressed against it at a specific load using a lever and weight, the experiment was conducted. Weights were taken before and after testing to determine the measure of occurred wear. A sample with diameter and length of 10 and 30 mm, respectively were used to make the counter disc. ASTM G99 standard was used to manage the wear test. The EN 31 Hardened steel sample has a diameter and thickness of 165 and 8 mm, respectively. A weighing balance that has a minimum count of 0.00001 g was used. Applying the weight difference method to calculate wear, the amount of wear was determined. Friction sensors were employed on pin-on-disc machines to measure frictional force. From the frictional force, coefficients of friction were calculated. Experiments were conducted based on the TaguchiL<sub>16</sub> (4<sup>4</sup>) orthogonal array. The detailed parameters are presented in Table1 and the WR and COF responses are presented in Table 2.

**Table 1**

Process parameters and their levels.

Weight percentage (wt.%)	0	3	6	9
Load (N)	5	10	15	20
Sliding distance (m)	500	750	1000	1250
Sliding velocity (m/s)	1.0	1.5	2.0	2.5

**Table 2**

Experimental details.

Exp. No	Wt.% of HA	P (N)	V (m/s)	D (m)	WR (mm <sup>3</sup> /m) $\times 10^{-3}$	COF	S/N ratio	S/N ratio
1	0	5	1.0	500	5.9611	0.34	-15.5065	9.3704
2	0	10	1.5	750	6.9876	0.55	-16.8866	5.1927
3	0	15	2.0	1000	9.5790	0.46	-19.6264	6.7448

4	0	20	2.5	1250	12.2797	0.64	-21.7838	3.8764
5	3	5	1.5	1000	8.8352	0.30	-18.9243	10.4576
6	3	10	1.0	1250	11.1980	0.53	-20.9828	5.5145
7	3	15	2.5	500	4.5144	0.41	-13.0920	7.8152
8	3	20	2.0	750	6.8376	0.57	-16.6981	4.8825
9	6	5	2.0	1250	10.3802	0.26	-20.3241	11.7005
10	6	10	2.5	1000	8.4110	0.50	-18.4970	6.0206
11	6	15	1.0	750	6.4286	0.39	-16.1623	8.2533
12	6	20	1.5	500	4.3214	0.53	-12.7124	5.5145
13	9	5	2.5	750	5.5208	0.22	-14.8400	13.1515
14	9	10	2.0	500	3.7701	0.45	-11.5270	6.9357
15	9	15	1.5	1250	9.6042	0.32	-19.6493	9.9333
16	9	20	1.0	1000	7.8088	0.49	-17.8516	6.1343

With experimental work, the disc was machined and lapped to make it and its surface smooth, respectively. Three samples of the composite were tested one after another, and the process was repeated three times. Both the top and bottom surfaces of the disc were cleaned with acetone before testing. The test was conducted under dry conditions without the use of lubricating oil. The surface roughness,  $R_a$  value achieved on disc sample was  $0.2 \mu\text{m}$ . The disc top and bottom surfaces were not lubricated with oil. The duration of the experiment, the load and the relative speed of the disc were kept constant, as well as the track diameter and rotation speed to maintain consistency. Wear experiments were conducted based on the data provided in Table 2.

Tangential force was measured from a linear variable differential transducer installed on the pin-on-disc machine. WR was calculated, using Eqs (1) and (2). Taguchi technique can be used to reduce the number of experiments, therefore it is an attractive method for improving process variables [43,49]. Taguchi-based S/N analysis was used to analyse experimental data. As minimum WR and COF were of interest, the smaller value was a better characteristics and was chosen. In addition, using Eqs (1) and (2), the smallest S/N ratio was selected to determine WR and COF [45,50].

$$\text{Wear rate} = \text{Mass loss} \times \text{Density} / D \text{ (mm}^3/\text{m)} \quad (1)$$

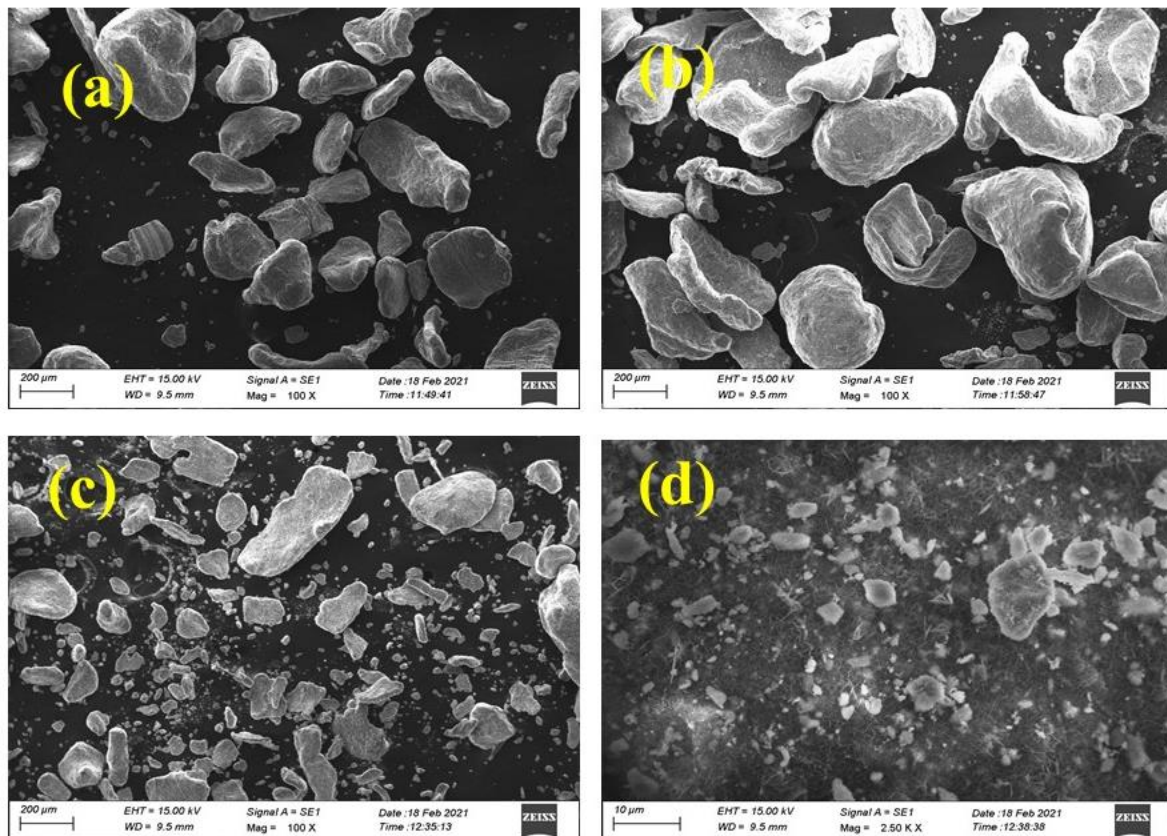
$$V = \Pi D N / 1000 \quad (2)$$

Eqn (2) Where  $V$  = Velocity (m/min),  $D$  = diameter (mm) and  $N$  = speed (rpm).

### 3. Results and discussion

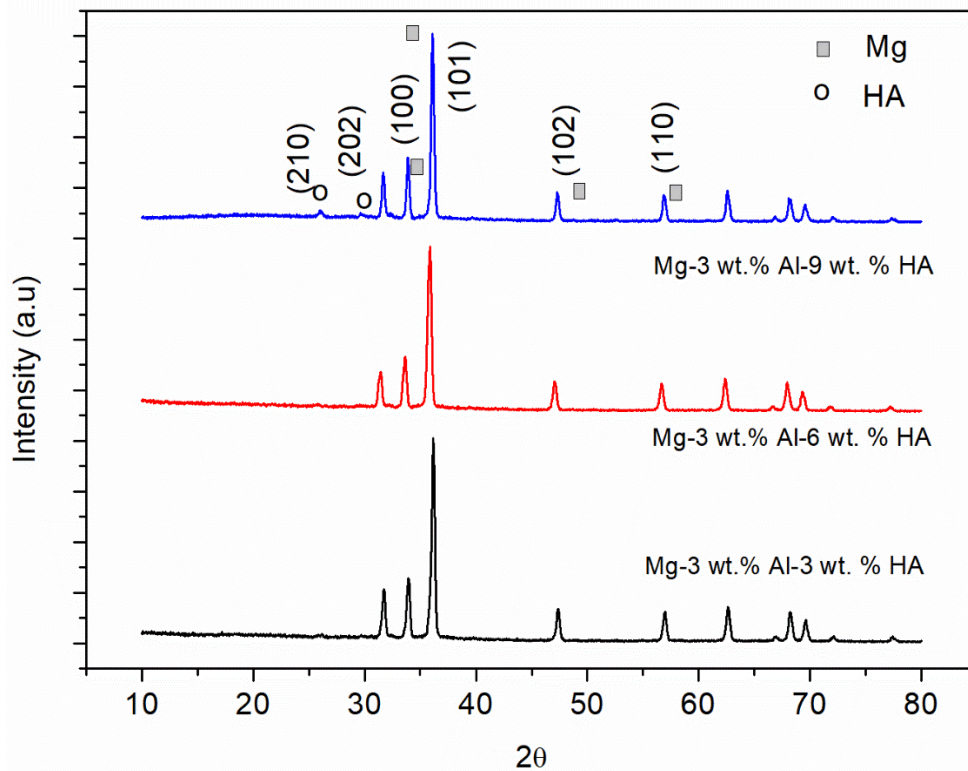
#### 3.1 Characterisation analysis of composite powders

SEM images in Figs 5(a-d) depict the powders of the various ball milled Mg3Al/HA composite samples. Particles of HA occupied a relatively uniform distribution within the matrix of Mg alloy. In all composite mixtures, the HA did not agglomerate. This can be attributed to the proper milling process. Figs 5(c) and (d) show that the Mg3Al/9HA mix contains more HA. This was obvious and indicated that a greater number of molecules of HA was present [14].



**Fig.5.** SEM images of the various ball milled Mg/3Al/HA powders: (a) Mg3Al/3HA, (b)Mg3Al/6HA, (c) and (d) Mg3Al/9HA.

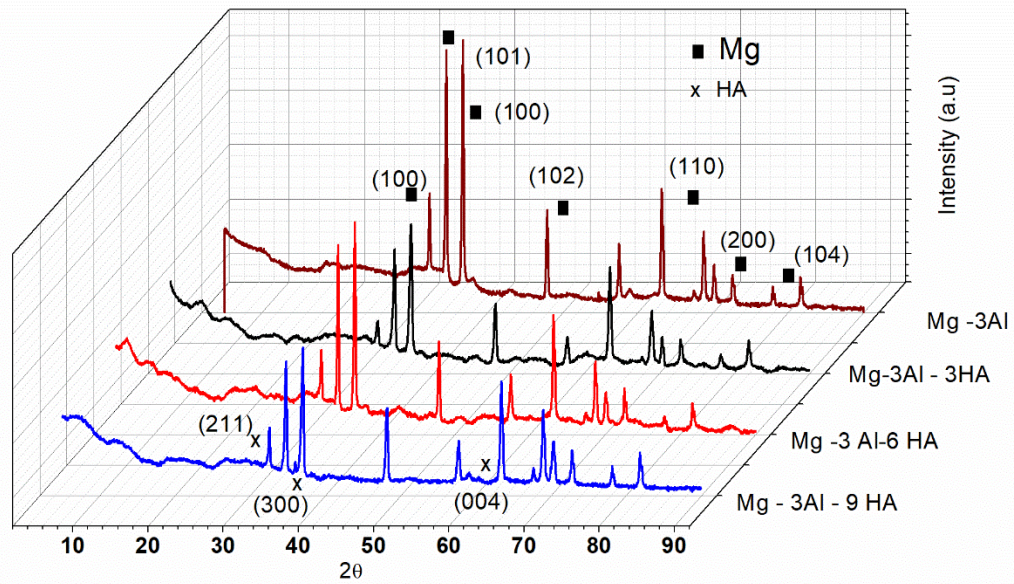
The graphical XRD pattern of Mg3Al/HA composite powders is shown in Fig. 6. Each plane was represented in the XRD pattern. As a result, Mg recorded the maximum peak in the pattern, while HA has the smallest and the Mg matrix was higher. A change in the Mg peak was observed, because of addition of HA to the Mg3Al matrix. In all compositions, it can be observed from their XRD patterns that HA was well incorporated to the Mg matrix. Mg and HA peak of XRD patterns were identified and indexed based on reported patterns: JCPDS No. 09-432 and 04-770 for HA and Mg, respectively.



**Fig. 6.** XRD pattern of Mg3Al/HA composite powders.

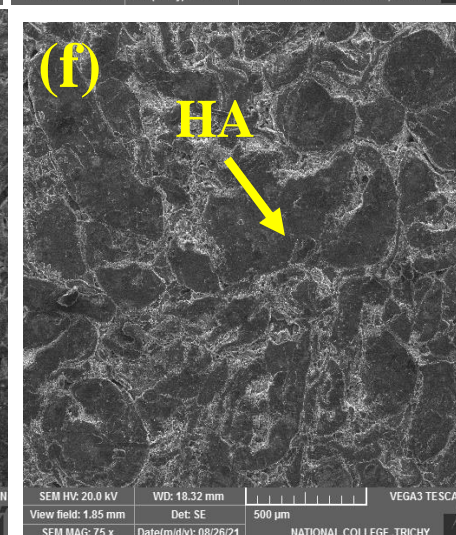
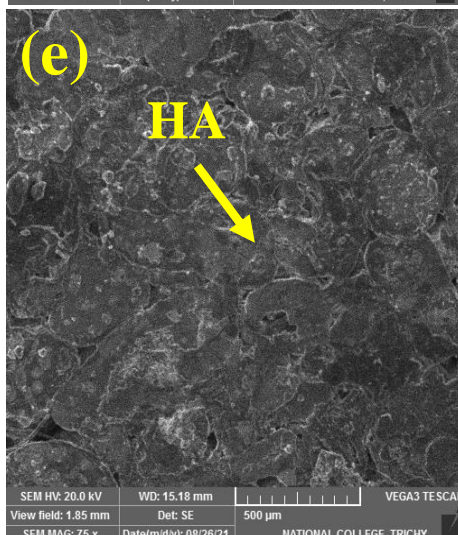
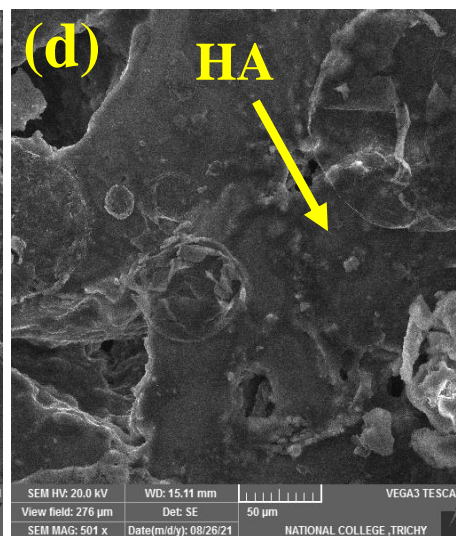
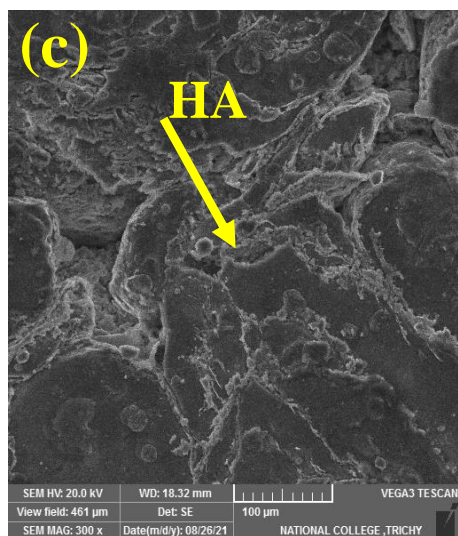
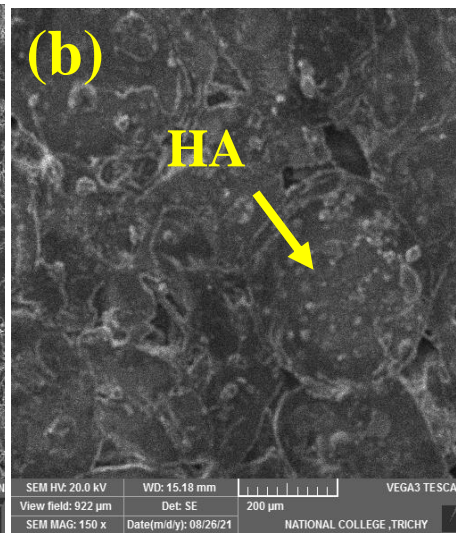
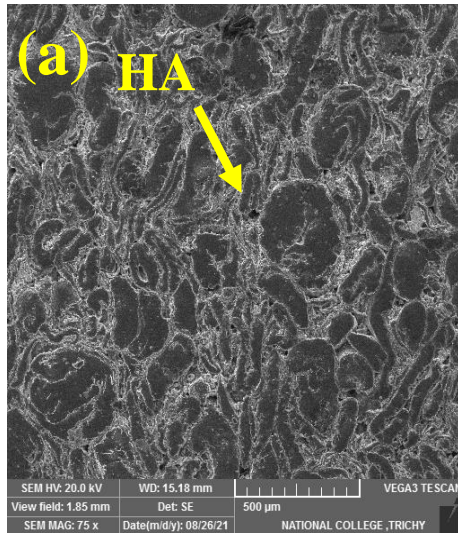
### 3.2 Characterisation analysis of sintered samples

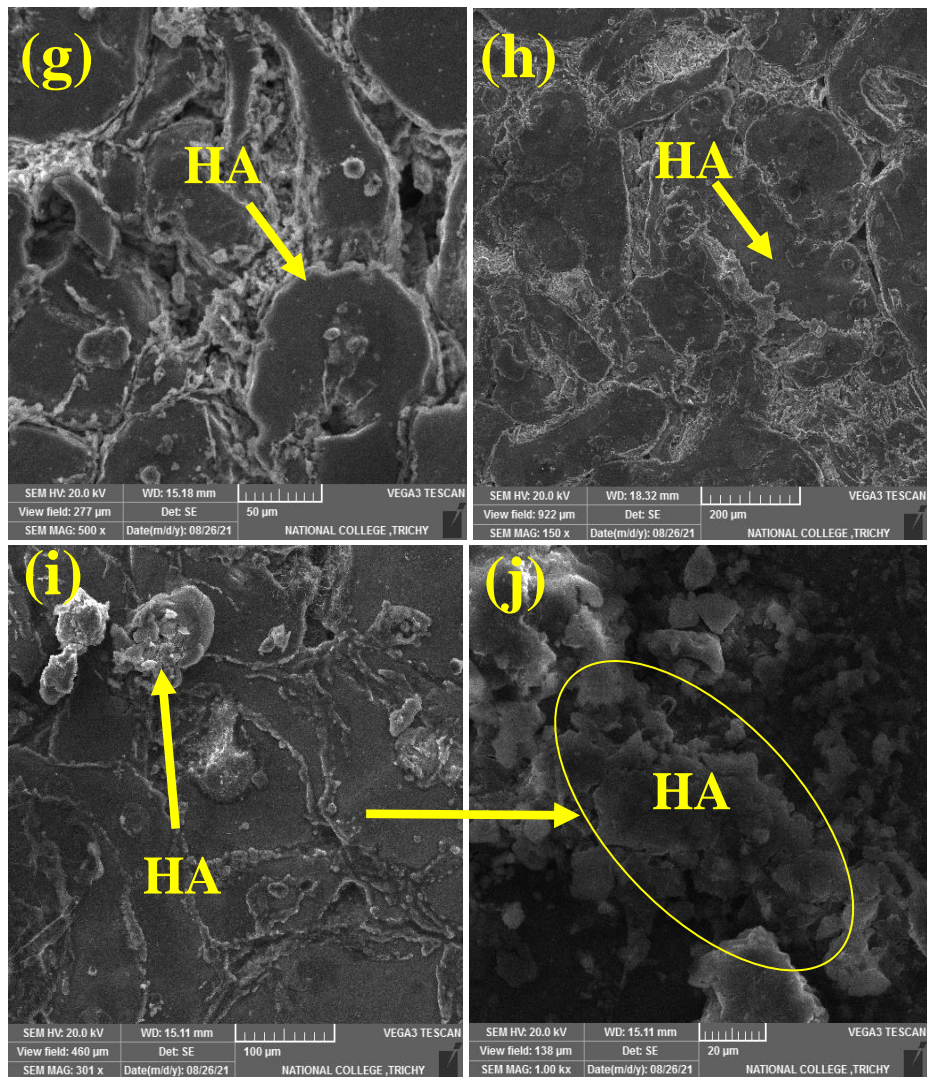
XRD pattern was obtained for sintered Mg3Al/HA composites sintered at 450°C (Fig. 7). Mg was identified as the major peak, while no peaks were obtained for Al, since a very low amount of Al (3 wt.%) was added as alloying element, as similarly reported [32]. It was evident that no impurities were created, due to the low melting temperature used during the sintering process. From the pattern, HA assured an appropriate bond between Mg and HA. By incorporating HA to the composite, a significantly increased in peak was observed for sample with 9 wt. % of HA.



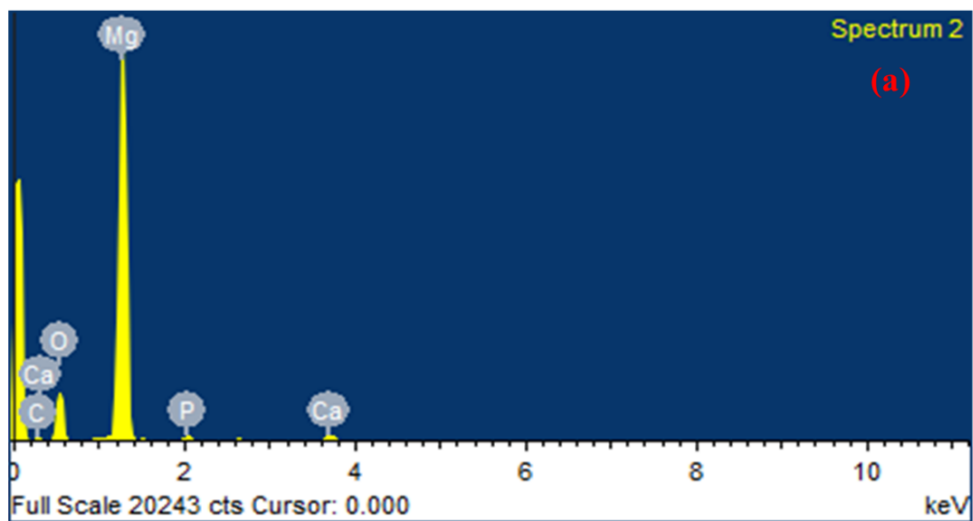
**Fig.7.** XRD pattern of Mg3Al/HAsintered composites.

Additionally, Figs 8 (a)-(j) depict the SEM micrographs of sintered Mg3Al/HA composites. The HA particles were evenly distributed in all the images. All the samples displayed good bonding between the HA particles and Mg matrix. It was observed that there was no agglomeration of the sample with more HA. A uniform distribution was achieved, because of the proper ball milling of Mg, Al and HA powders [2]. As shown in Figs 9(a-c), energy dispersive X-ray spectroscopy (EDS) analysis was conducted on HA reinforced Mg3Al alloyed composite samples. As expected, the Mg and HA peak were significantly visible or very clear and small size of peak showed the Al element in Figs 9(b) and (c).





**Fig. 8.** SEM images of sintered (a-c) Mg<sub>3</sub>Al/3HA, (d-f) Mg<sub>3</sub>Al/6HA and (g-j) Mg<sub>3</sub>Al/9HA composites.



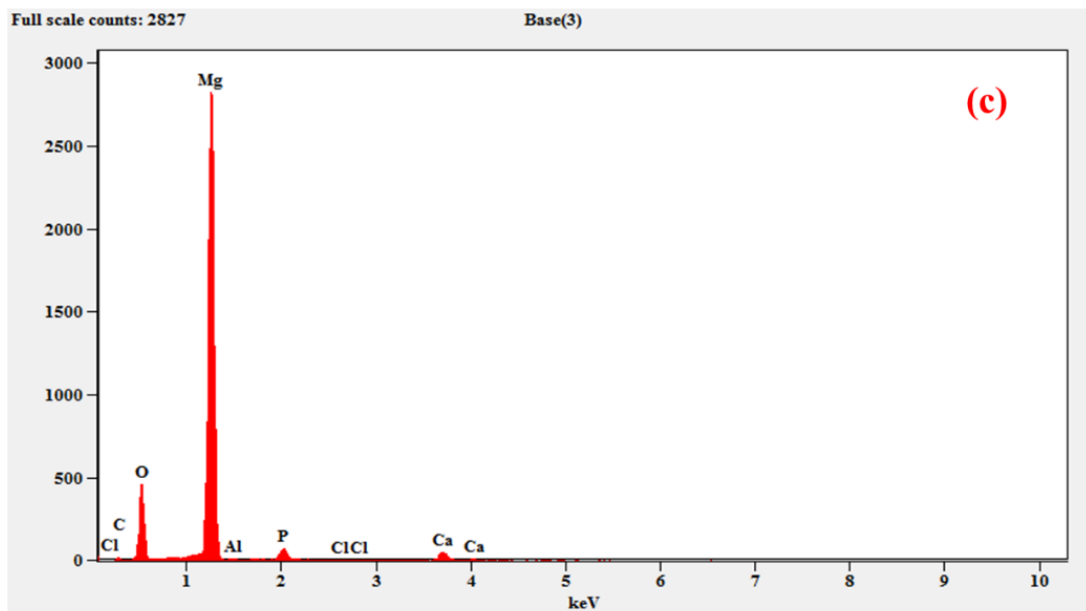
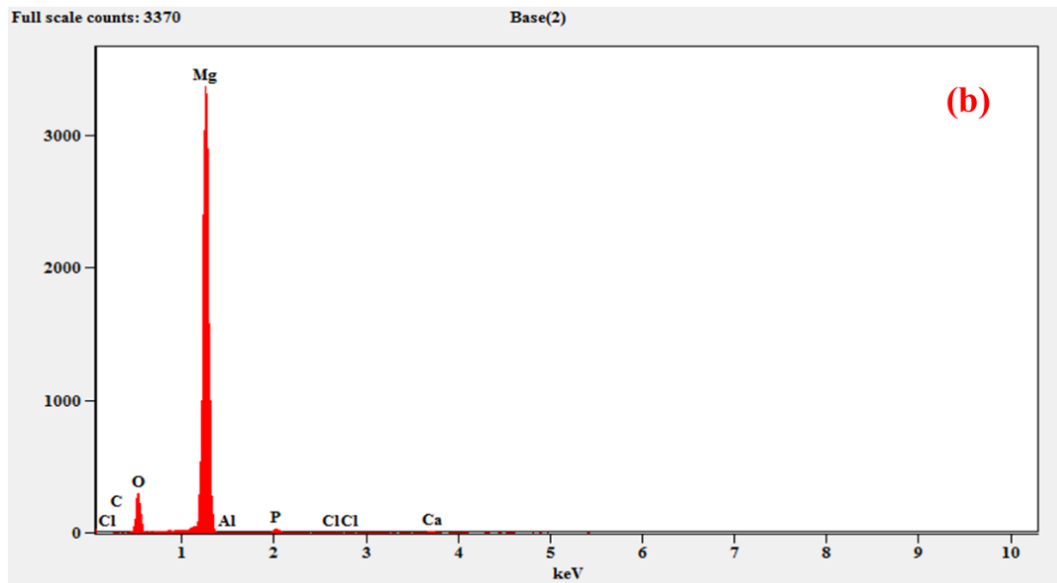
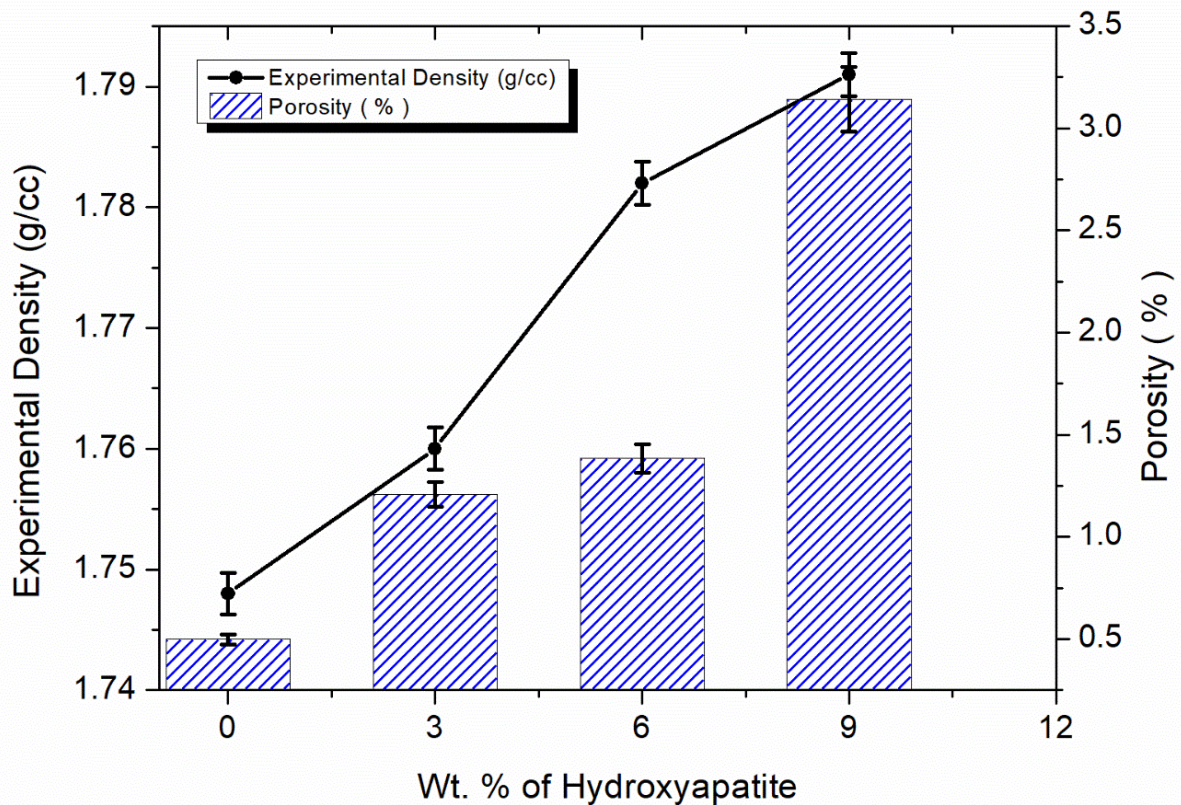


**Fig. 9.** EDS images of sintered (a) Mg<sub>3</sub>Al/3HA, (b) Mg<sub>3</sub>Al/6HA and (c) Mg<sub>3</sub>Al/9HA composites.

### 3.3 Properties of Mg<sub>3</sub>Al/HA sintered composites

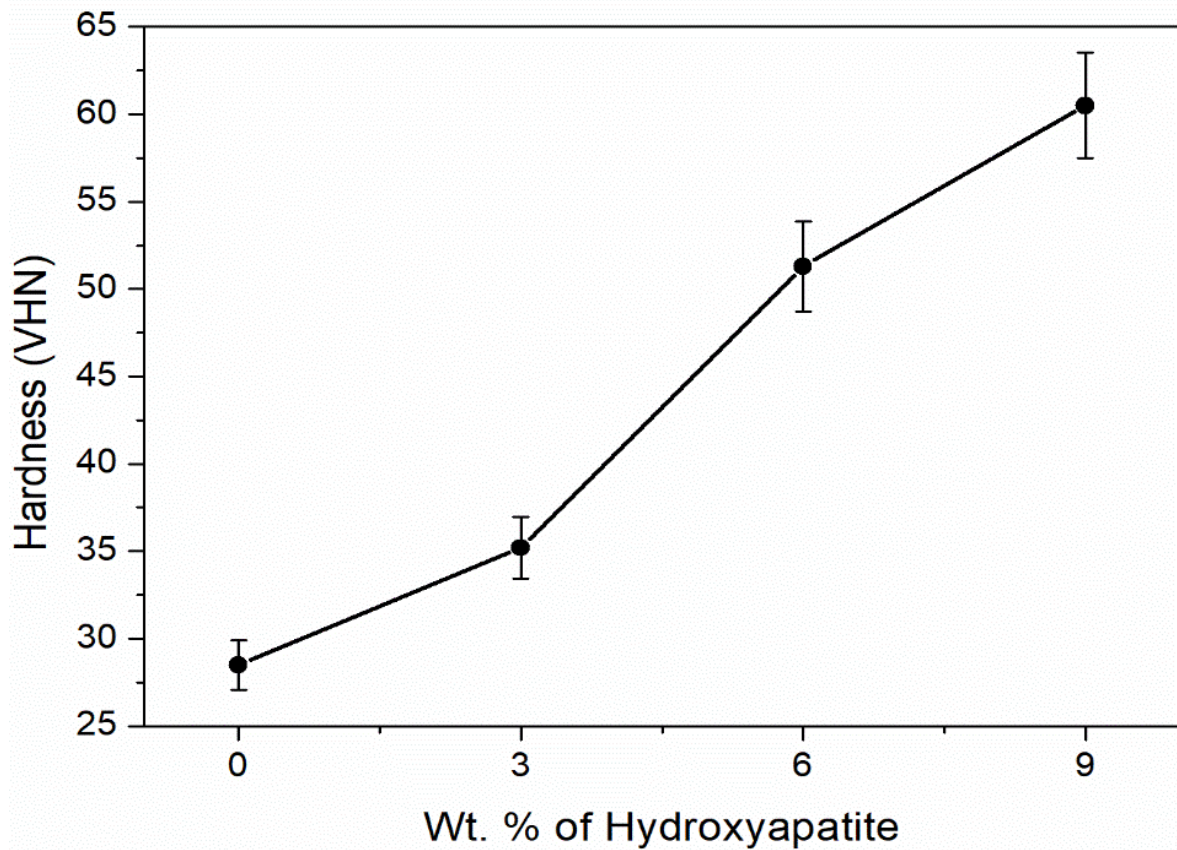
From Fig. 10, the effects of HA inclusion on the density of Mg<sub>3</sub>Al/HA composites are shown. The densities of both experimentally produced and theoretical samples were increased, as the wt.% of HA in Mg alloy matrix increased. The theoretical densities of all the samples were greater than that of the experimental densities. The porosity increased with an increase in the wt.% of HA particles in the Mg<sub>3</sub>Al matrix. Sintered samples typically

recorded a higher density than green composites, because the bonds between the particles were improved during the sintering process and voids were eliminated. In addition, during the heating process, moisture from the samples was removed [12].



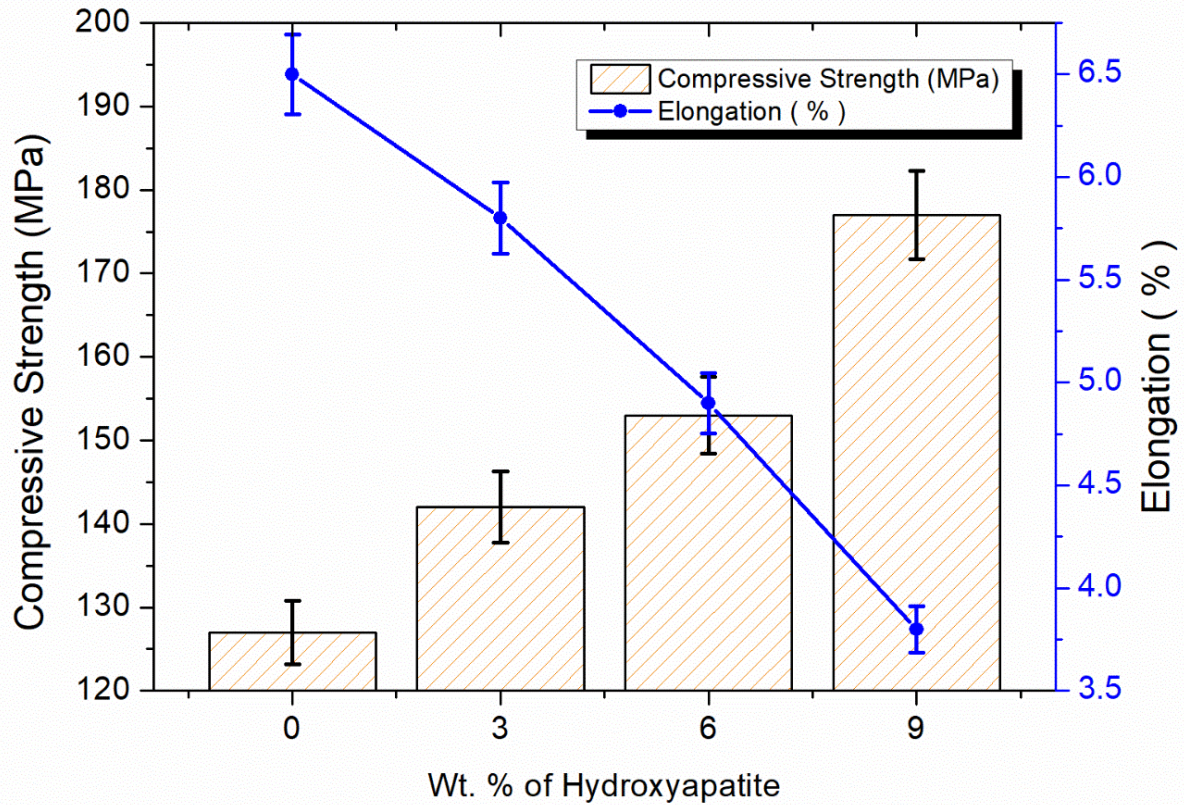
**Fig. 10.** Effects of HA on the densities of the various composites.

Fig. 11 shows the hardness of the base alloy and its composite reinforced with HA. The hardness of the composite was higher than the base Mg3Al matrix alloy. The incorporation of HA to the Mg alloy matrix enhanced the hardness of the sintered Mg3Al/HA composites. The hardness of HA was higher than the Mg and its alloys. Hence, the higher hardness of HA was responsible for the increase in hardness of the composite samples [2]. The increase in quantity of HA in the matrix increased the hardness and influenced the sintered samples to be too brittle. The highest hardness was acquired for the sample with 9 wt.% of HA. This present study considered the highest 9 wt.% of HA, since beyond this threshold value, the sample became too brittle and the mechanical properties deteriorated.



**Fig. 11.** Effects of HA on the hardness of the various composites.

Moving forward, Fig. 12 depicts the compressive strengths of the HA reinforced Mg3Al matrix composites and base alloy. The compressive strength was improved, due to the inclusion of HA to the matrix. The improved strength can be further attributed to the following factors: (i) incorporation of hard HA particles to the Mg3Al matrix, (ii) uniform distribution of HA within the metal matrix, (iii) thermal mismatch between the HA particles and Mg3Al alloy during sintering process and (iv) grain refinement, due to the presence of HA particles [3]. The highest compressive strength of 177 MPa was observed with sample of 9 wt.% HA. The base Mg3Al alloy recorded the lowest value of 127 MPa.



**Fig. 12.** Effects of HA on the compressive strengths and elongations of the various composites.

Fig. 13 shows the weight loss (mm/year) and corrosion rate for Mg3Al alloys and Mg3Al/HA composites during salt spray test. The inclusion of HA to the Mg3Al alloy decreased the weight loss. Additionally, the corrosion rate (mm/year) also decreased, as the Mg3Al matrix contained a higher wt.% of HA. The composite samples showed a higher corrosion resistance. HA was distributed in the grain boundary of the matrix and generated layer to provide passive corrosion protection.

The immersion and salt spray tests established that Mg corrosion appeared identically. Among the nonferrous alloys, Mg is a good option for biomedical field. Bakhsheshi-Rad et al. [51] reported that the chloride iron, on the other hand, corroded quite smoothly. Adding ceramic/oxide particles to the matrix of Mg alloys could boost the corrosion resistance. Using the dissimilar microstructures in the composites, corrosion resistance was greatly enhanced.

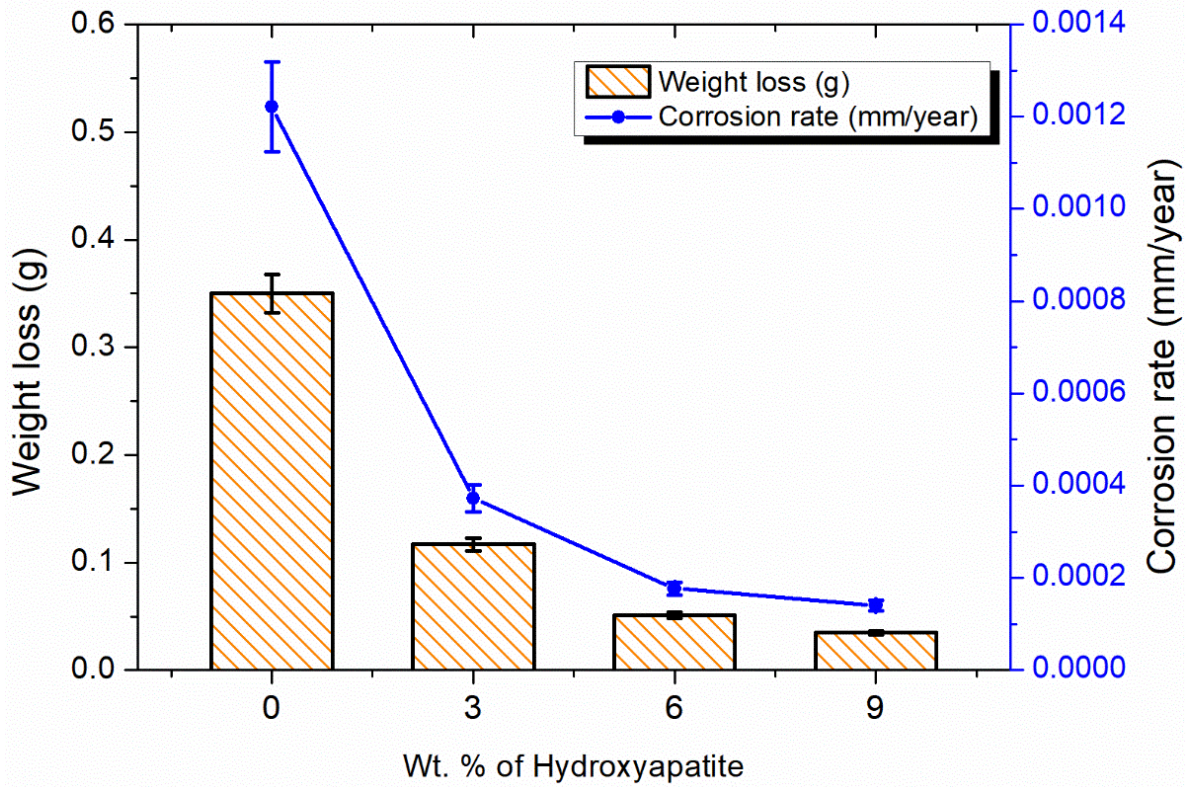


**Fig. 13.** Effects of HA on the corrosion behaviours of the various composites.

### 3.4 Wear analysis of Mg3Al/HA composites

Figs 14 and 15 depict the S/N ratio and mean plots for the WR, respectively. To achieve the lowest WR, it was observed that the combined parameters of A<sub>4</sub>B<sub>3</sub>C<sub>2</sub>D<sub>1</sub> represented the optimum value of reinforcement at Level IV (9 wt.%), V at Level III (2 m/s), D at Level II (750 m) and Pat Level I (5 N). Figs 16 and 17 show the S/N ratio and mean plot for the COF, respectively. During the analysis, it became apparent that the most optimal combined parameters to achieve minimal COF were A<sub>4</sub>B<sub>1</sub>C<sub>2</sub>D<sub>1</sub>, which means that value of reinforcement at Level IV (9 wt.%), V at Level I (1 m/s), D at Level II (750 m) and Pat Level I (5 N). Tables 3-6 present the S/N ratio and mean values for the WR and COF.

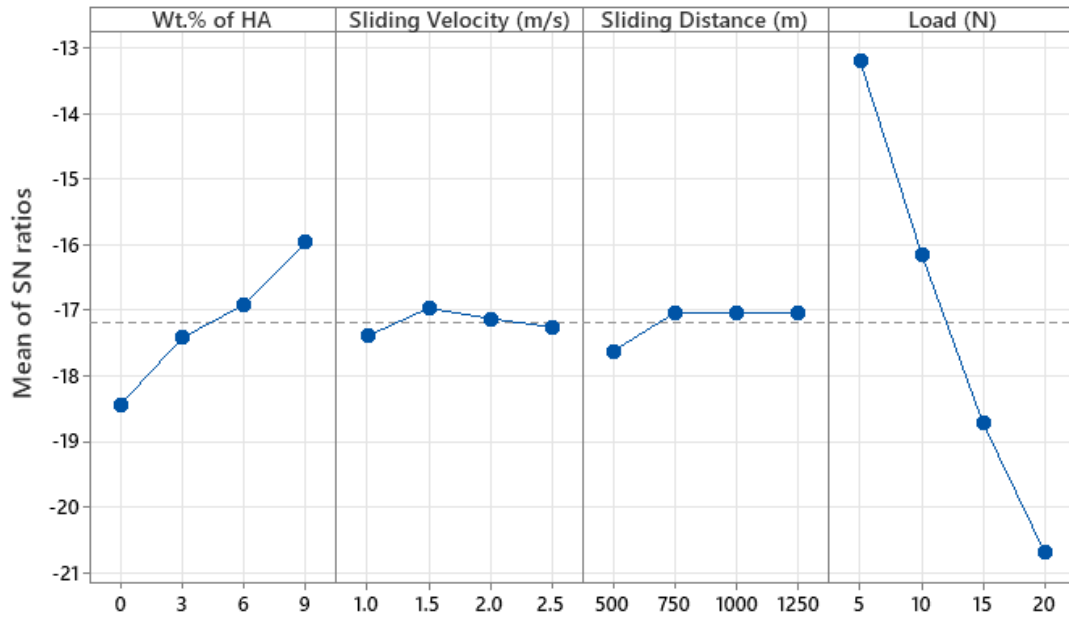


**Fig. 14.** S/N ratio plot of WR.

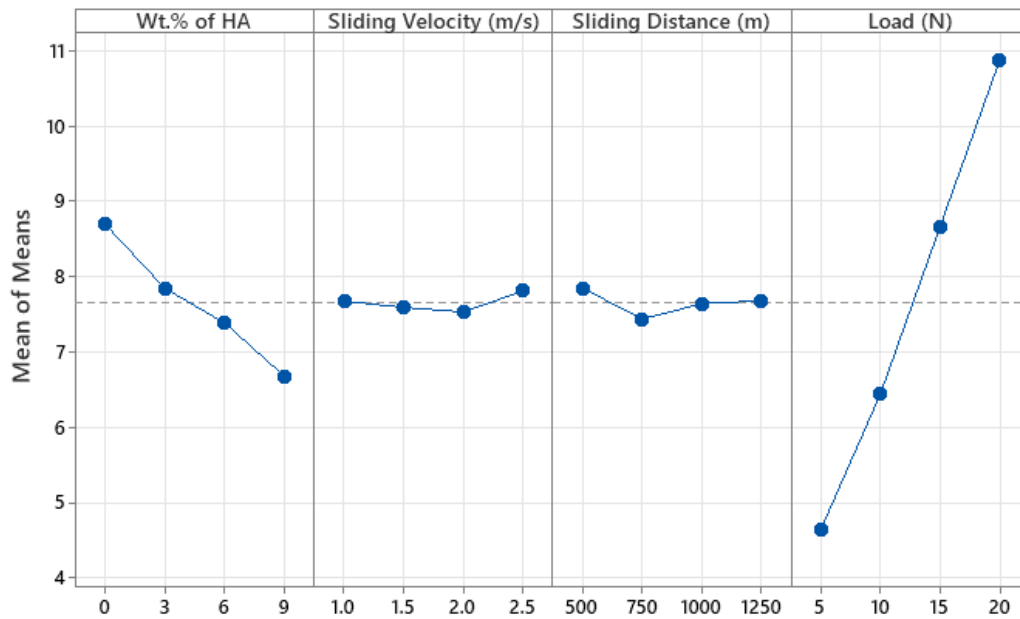


**Fig. 15.** Mean plot of WR.

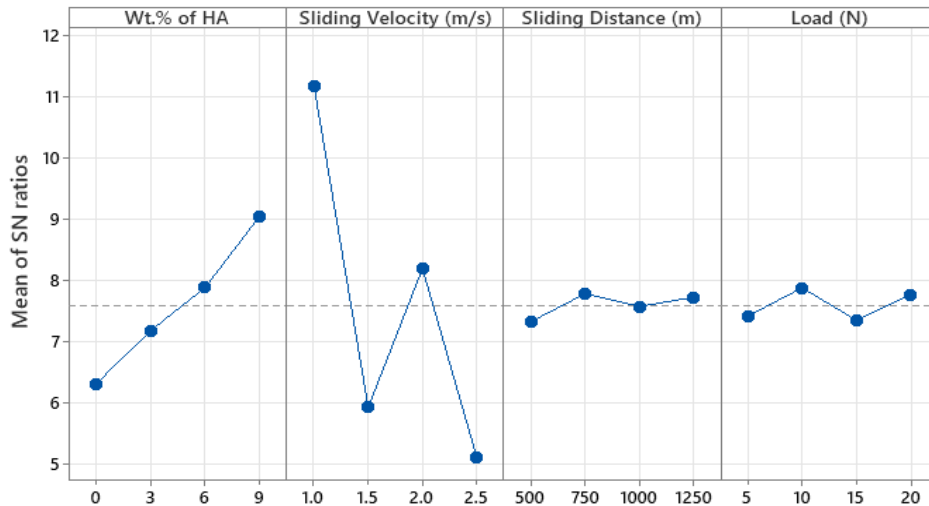


**Fig. 16.** S/N ratio plot of COF.

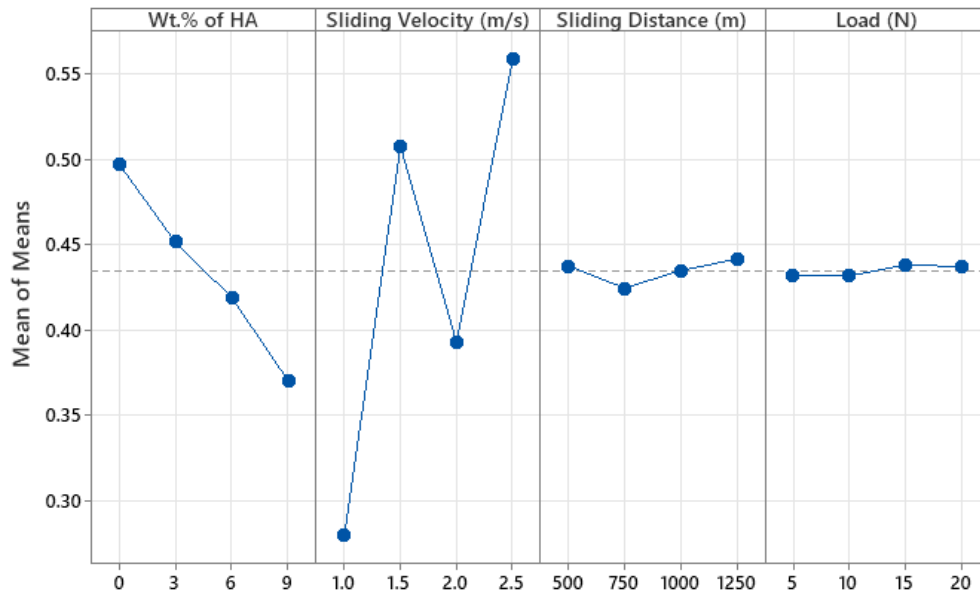


**Fig. 17.** Mean plot of COF

**Table 3**

Response table for S/N ratios for WR.

Level	Wt.% of HA	V (m/s)	D (m)	P (N)
I	-18.45	-17.40	-17.63	-13.21
II	-17.42	-16.97	-17.04	-16.15
III	-16.92	-17.13	-17.04	-18.72
IV	-15.97	-17.26	-17.05	-20.68
Delta	2.48	0.43	0.58	7.48
Rank	2	4	3	1

**Table 4**

Response table for means for WR.

Level	Wt.% of HA	V(m/s)	D(m)	P (N)
I	8.702	7.674	7.849	4.642
II	7.846	7.592	7.437	6.444
III	7.385	7.532	7.642	8.659
IV	6.676	7.812	7.681	10.866
Delta	2.026	0.280	0.412	6.224
Rank	2	4	3	1

**Table 5**

Response table for S/N ratios for COF.

Level	Wt.% of HA	V(m/s)	D(m)	P (N)
I	6.296	11.170	7.318	7.409
II	7.167	5.916	7.775	7.870
III	7.872	8.187	7.566	7.339
IV	9.039	5.102	7.716	7.756
Delta	2.743	6.068	0.456	0.531
Rank	2	1	4	3

**Table 6**

Response table for means for COF.

Level	Wt.% of HA	V(m/s)	D(m)	P (N)
I	0.4975	0.2800	0.4375	0.4317
II	0.4517	0.5075	0.4247	0.4317
III	0.4192	0.3930	0.4350	0.4384
IV	0.3705	0.5584	0.4417	0.4372
Delta	0.1270	0.2784	0.0170	0.0067
Rank	2	1	3	4

According to Tables 3-6, the applied load recorded the greatest impact on the WR and the reinforcement had the greatest impact on the COF. According to the Archard's law, the applied load between the contacting surfaces determined the volume of WR. Through application of load, the sample remained continuously in contact with the load, causing damage to the surface and resulting to a volumetric wear [52]. Due to the increased contact pressure, the WR of the pin surface and the counter disc was faster as the load applied increased. While comparing composite samples with unreinforced matrix alloys, it appeared that the composite samples exhibited a lesser WR.

In addition, the particles of HA increased the hardness of the composite, which reduced COF and WR. Contact with opposing surfaces blunt and smoothed out the protrusions of reinforcement particles at the initial conditions of sliding. A reduction of COF and WR was observed by smoothing the reinforcement particles and increasing the sliding distance. This led to the evolution of a self-lubricating layer on the reinforcement particles. When the sliding distance by an unreinforced matrix alloy increased, due to an increase in surface temperature, less material was retained. This resulted to greater wear rates. By virtue of its higher hardness, composites have better wear resistance at a higher sliding distance than unreinforced matrix alloys. Generally, as the sliding velocity increased, the friction between the surfaces increased, causing the interfacial temperature to rise. The high temperature of the alloy matrix accelerated the oxidation process, causing a thick layer of oxides to form, which were the mechanically mixing layers [54]. The development of an oxide layer enhanced the wear resistance of the mating surfaces by allowing them to slide smoothly. The lesser shear strength tribofilms on the rubbing surfaces occurred, because of the high sliding velocity and increased surface temperature between the rubbing surfaces, since the friction coefficient decreased. The composites surface formed a tribo layer at low sliding speeds, which has the effect of reducing tangential friction.

Figs 18-20 depict the contour plots for WR. The plot in Fig. 18 shows the effect of P and wt.% HA on WR. According to the plot drawn in blue, the decrease in WR can be observed on the right side corner, as an effect of an increase in wt.% of HA. Fig.19 depicts the same trend as Fig.18, considering the P and D. The dotted red line on Fig.20 shows how an increase in the wt.% of reinforcement caused an increase in the WR, as observed from the interaction between wt.% of HA and D. With this plot, the interaction between two parameters for the WR can be clearly observed.

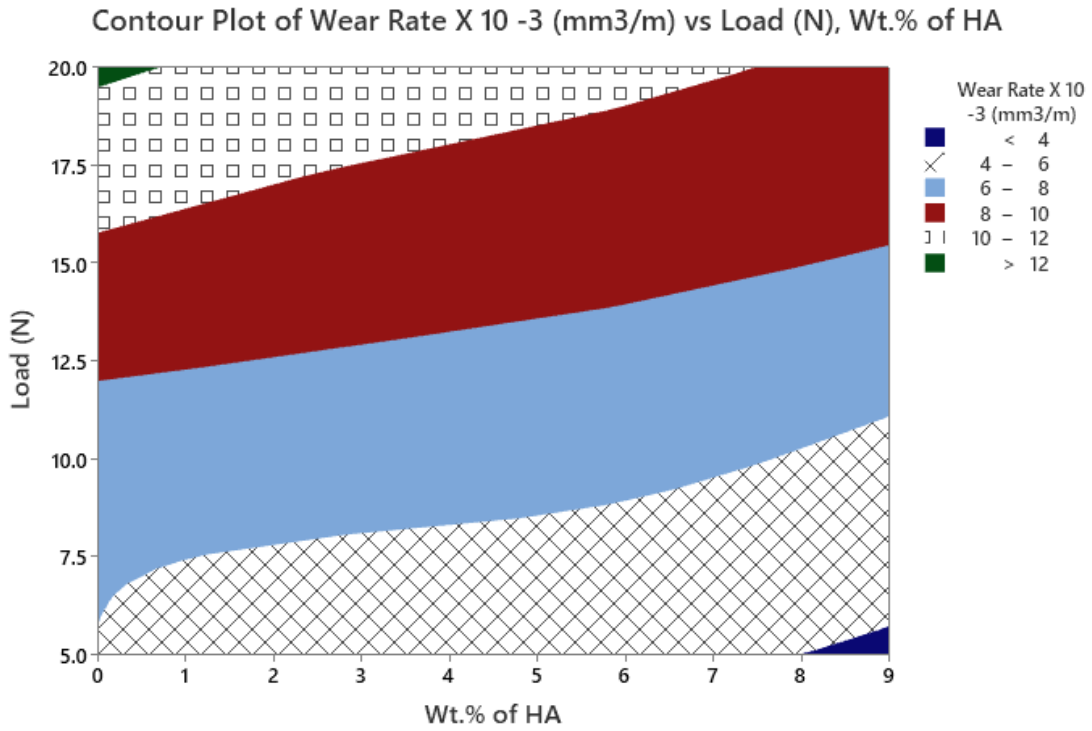


Fig. 18. Contour plot for WR.

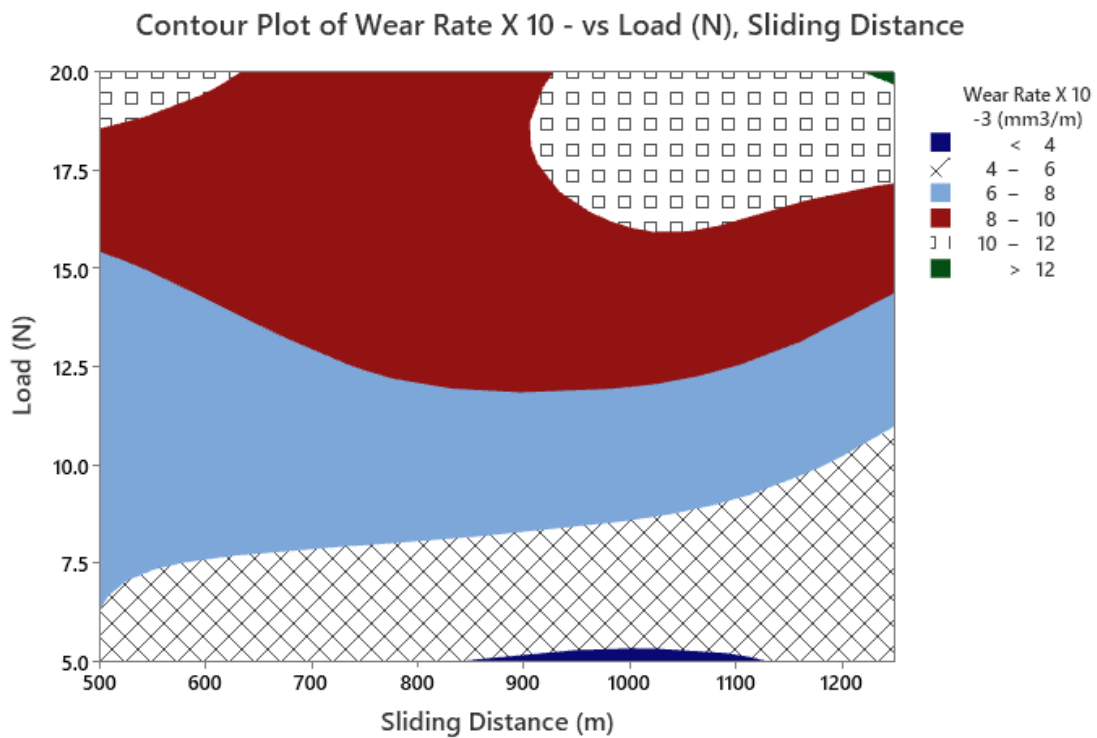
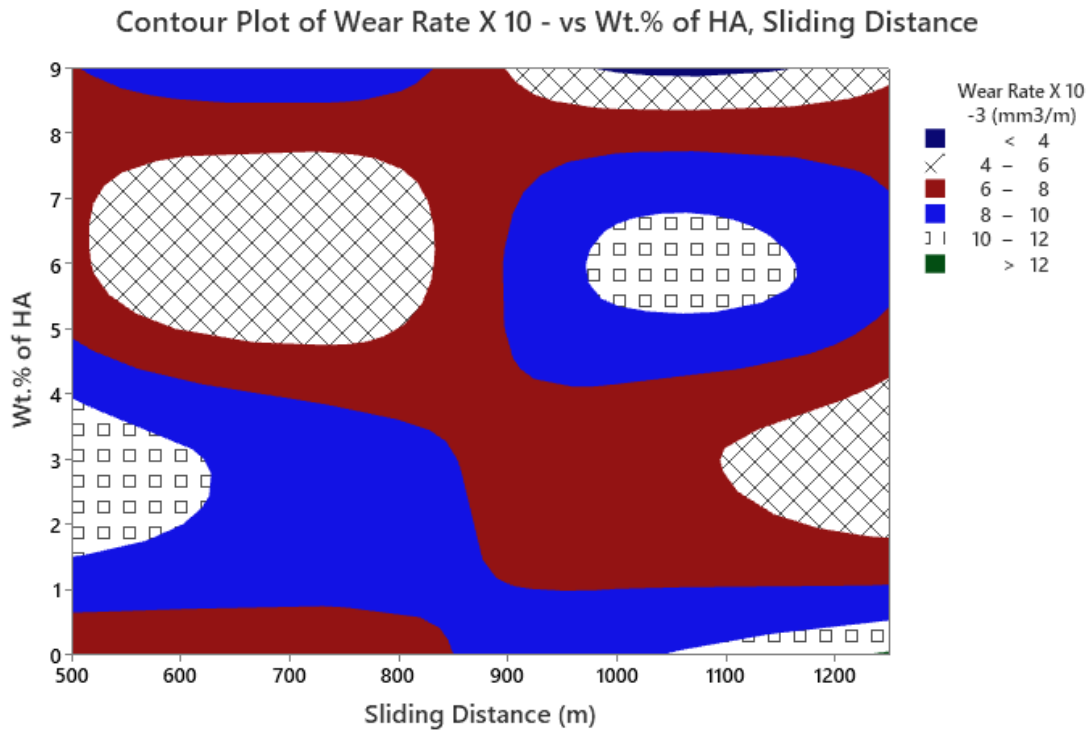
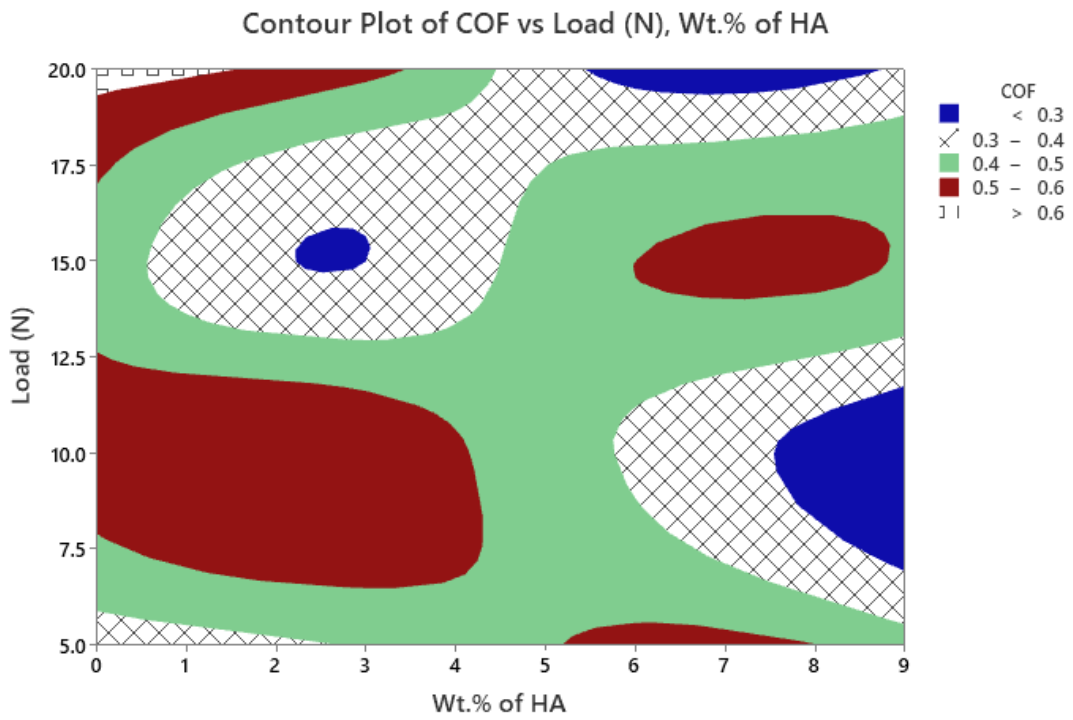


Fig. 19. Contour plot for WR.



**Fig. 20.** Contour plot for WR.

Similarly, the contour plots of the COF are shown in Figs 21-23: *P* versus wt.% of HA; *P* versus *D* and wt.% of HA versus *D*, respectively. When the composites were tested under wear, the COF increased as the load was increased. From Fig. 22, it was evident from the increase in applied load that the COF increased. Considering Fig.23, it was significantly observed that the increased wt.% of HA and the increased sliding distance caused friction on the composite surface during dry sliding conditions. As a result of the above factors, the proposed materials were more resistant to wear, due to their increased wt.% of HA content in the matrix alloy. Hence, they acted as wear resistant materials, because of their hard nature [52-54].



**Fig. 21.** Contour plot for COF.

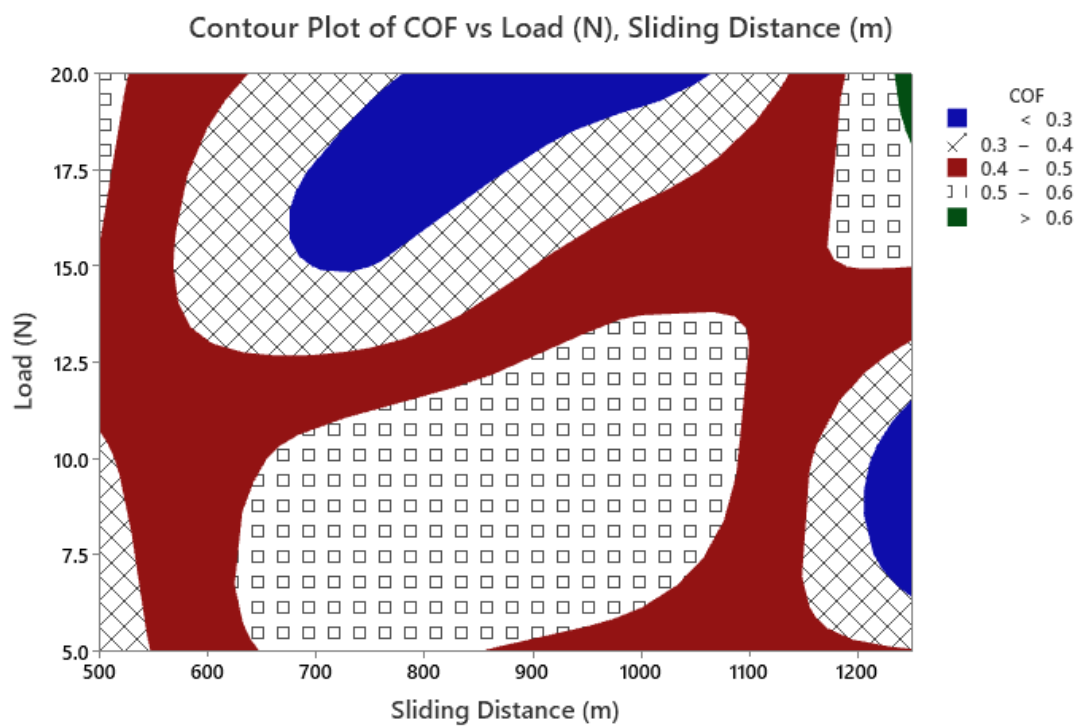


**Fig. 22.** Contour plot for COF.

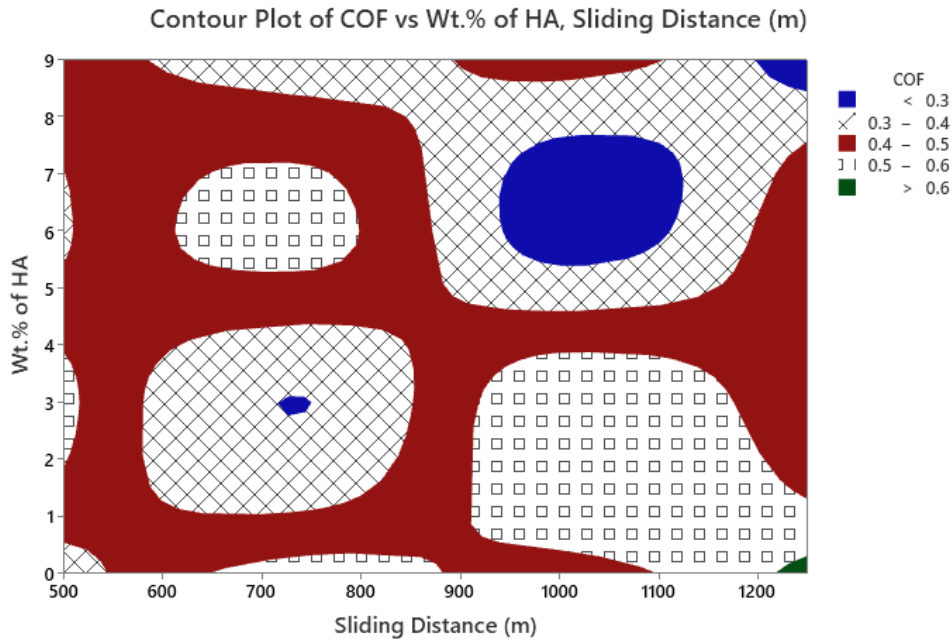


**Fig. 23.** Contour plot for COF.

Analysis of variance (ANOVA) was conducted to determine the percentage contribution of parameters, such as wt.% of HA, P, V and D to WR and COF of the Mg3Al/HA composites. Table 7 presents the ANOVA for WR. Based on the F-value, it can be observed that the value of P was the most dominant factor, followed by the reinforcement and sliding distance. ANOVA results on COF are presented in Table 8. By analysing the data presented in Table 8, it was evident that the V was the most influencing factor, followed by the HA content, D and P. Eqs (3) and (4) present the regression models for WR and COF, respectively [53]. Figs 24 and 25 show the probability plots for WR and COF, respectively. Evidently, the errors were within the limit, according to 95% confidence interval.

**Table 7**

ANOVA for WR.

Source	DF	Adj SS	Adj MS	F-value	P-value
Wt.% of HA	3	8.6551	2.8850	25.06	0.0126
V (m/s)	3	0.1768	0.0589	0.51	0.7019
D (m)	3	0.3440	0.1147	1.00	0.5012
P (N)	3	87.4467	29.1489	253.23	0.0004
Error	3	0.3453	0.1151		
Total	15	96.9679			

**Table 8**

ANOVA for COF.

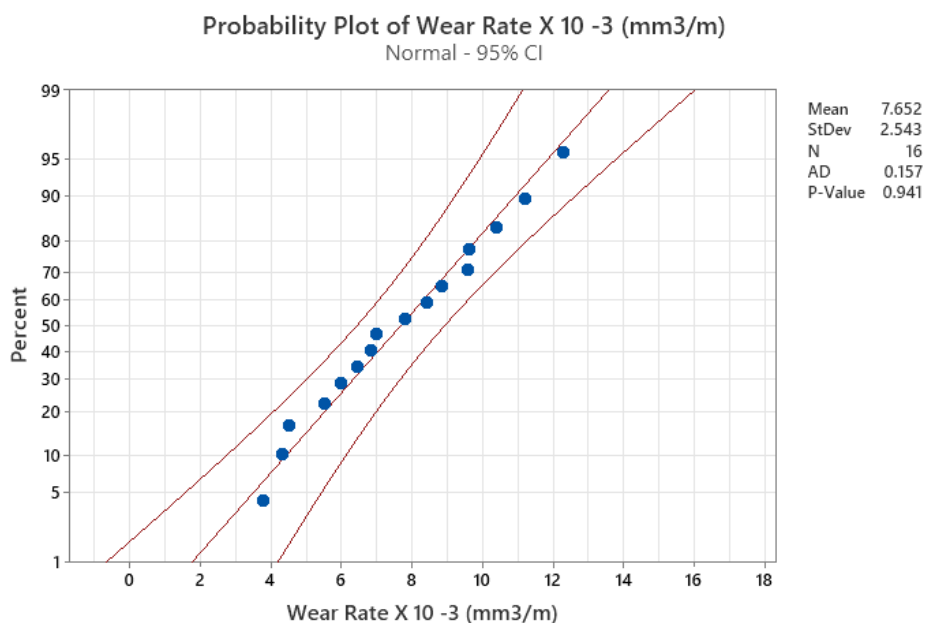
Source	DF	Adj SS	Adj MS	F-value	P-value
Wt.% of HA	3	0.034357	0.011452	58.29	0.0037
V (m/s)	3	0.185065	0.061688	313.96	0.0003
D (m)	3	0.000629	0.000210	1.07	0.4791
P (N)	3	0.000152	0.000051	0.26	0.8525
Error	3	0.000589	0.000196		
Total	15	0.220793			

*Regression equation for WR*

$$\text{Wear rate } \times 10^{-3} \left( \frac{\text{mm}^3}{\text{m}} \right) = 7.6523 + 1.050 A_1 + 0.194 A_2 - 0.267 A_3 - 0.976 A_4 + 0.022 B_1 - 0.061 B_2 - 0.121 B_3 + 0.160 B_4 + 0.197 C_1 - 0.215 C_2 - 0.011 C_3 + 0.029 C_4 - 3.011 D_1 - 1.209 D_2 + 1.006 D_3 + 3.213 D_4(3)$$

*Regression Equation for COF*

$$\text{COF} = 0.43472 + 0.06278A_1 + 0.01695A_2 - 0.01555 A_3 - 0.06418 A_4 - 0.15472 B_1 + 0.07278 B_2 - 0.04172 B_3 + 0.12366 B_4 + 0.00282 C_1 - 0.01005 C_2 - 0.00028 C_3 + 0.00695 C_4 - 0.00305 D_1 - 0.00305 D_2 + 0.00366D_3 + 0.00245 D_4(4)$$

**Fig. 24.** Probability plot of WR.

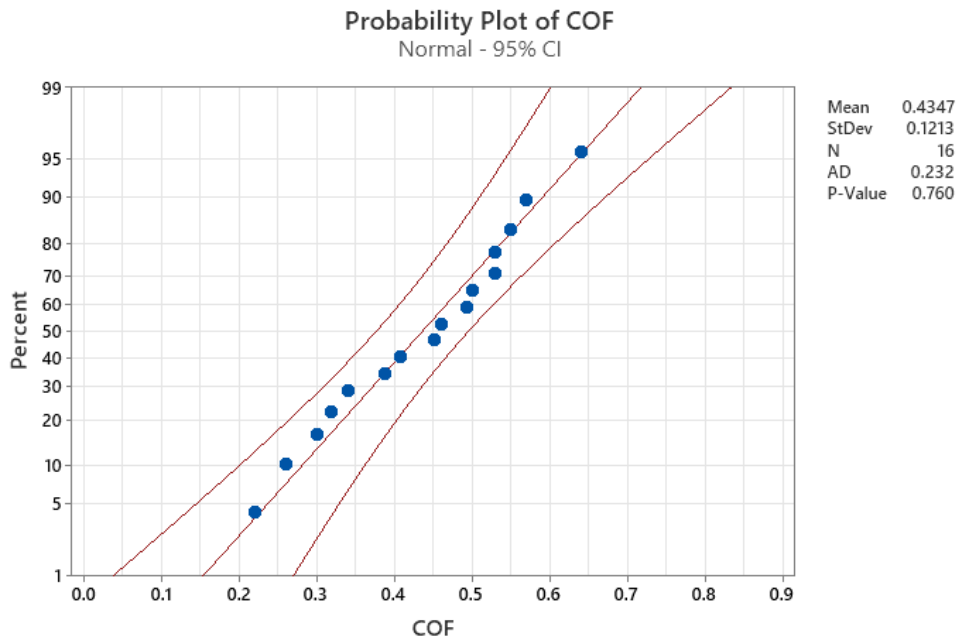


**Fig. 25.** Probability plot of COF.

### 3.5 Worn surface analysis

Figs 26–(a)-(h) depict the SEM images of the worn surfaces of the Mg3Al alloy and various Mg3Al/HA composite samples. Figs 26–(a) and (b) show the unreinforced alloy surface with repair of bluntly impaired regions, blister wear and huge flow of material with a lateral shift, caused by heavy plastic deformation. While, Figs 26(c) and (d) depict the formation of small cavities and cracks on the surface of the wear track, which suggested adhesive wear among the matrix alloys. From these graphs, it can be observed that a wear track formed on the head surface of the composites [55]. On this surface, it can be further observed that rigid and hollow formed much more shallowly in the composites than they did in unreinforced alloys, which resulted to the presence of reinforcement particles in the matrix materials. Figs 26–(c)-(h) show the HA contents of 6 and 9\_wt.% in the worn surface of the composite. However, there were some wear debris that accumulated on the wear track. This indicated that the wear was abrasive, due to the presence of HA particles in the composites. Due to the presence of HA particles, the deformed plastic shrinkage was reduced significantly, as the HA particles acted as a limitation to the displacements, thereby increased the wear resistance. When HA increased, both WR and COF decreased [52].

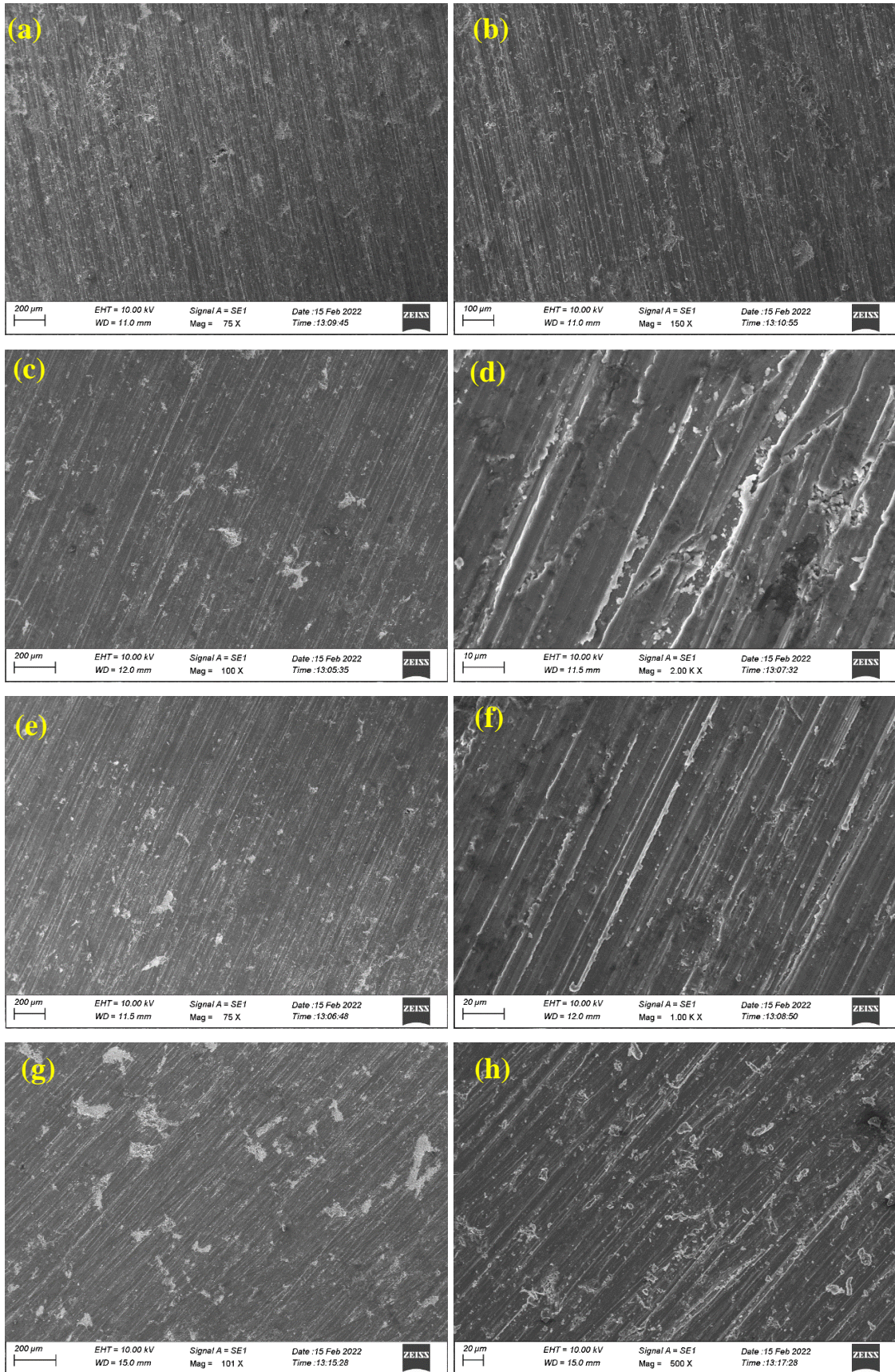


**Fig. 26**(a)-(h) Worn surface morphology of the (a,b) Mg3Al/HA, (c,d) Mg3Al/3HA, (e,f) Mg3Al/6HA and (g,h) Mg3Al/9HA composite samples.

#### 4. Conclusions

Base Mg<sub>3</sub>Al alloy and Mg<sub>3</sub>Al/HA composites samples with various 0, 3, 6 and 9 wt.% of HA contents have been successfully fabricated, using PM technique. Microstructure, mechanical and corrosion properties of the samples were well studied, including WR and COF. Summarily, the following points can be deduced from the results obtained:

- SEM analysis of Mg<sub>3</sub>Al/HA composite powders and sintered samples revealed the uniform distribution of HA matrix. Ball milled and sintered composites were analysed by XRD for matrix and reinforcing peaks, and established the absence of intermetallic phases.
- Addition of HA to the Mg<sub>3</sub>Al matrix enhanced the compressive strength, micro hardness and corrosion resistance of the composite with 9 wt.% of HA loading. The highest compressive strength of 177 MPa was recorded by the sample with 9 wt.% of HA, while the base Mg<sub>3</sub>Al alloy exhibited the lowest value of 127 MPa.
- The composite samples exhibited an abrasive wear mechanism and adhesive wear was observed with the Mg<sub>3</sub>Al samples, when SEM was used to conduct worn surface analysis.
- From S/N ratio analysis, the lowest WR was obtained with combined optimal parameters of A<sub>4</sub>B<sub>3</sub>C<sub>2</sub>D<sub>1</sub> with 9 wt.%, 2 m/s, 750 m and 5 N. Similarly, the optimal parameters for minimal COF were 9 wt.%, 1 m/s, 750 m and 5 N, as exhibited under combined parameters of A<sub>4</sub>B<sub>1</sub>C<sub>2</sub>D<sub>1</sub>.

Finally, various efficient applications of the Mg<sub>3</sub>Al alloy as well as Mg<sub>3</sub>Al/3HA, Mg<sub>3</sub>Al/6HA and Mg<sub>3</sub>Al/9HA composite samples should depend on their optimum wt.% of constituents, properties, working conditions/parameters and performances. Therefore, the aforementioned results contribute to the tribological knowledge required in the thriving field of composite technology.

#### Acknowledgments

The authors thankfully acknowledge the financial support provided by The Institution of Engineers, India.

## References

- [1] I. Dinaharan, S. Zhang, G. Chen, Q. Shi, Development of titanium particulate reinforced AZ31 magnesium matrix composites via friction stir processing, *J. Alloys Compd.* 820 (2020) 153071. <https://doi.org/10.1016/j.jallcom.2019.153071>
- [2] S. Jaiswal, Manoj Kumar, R. Pallavi Gupta, M. Kumaraswamy, Partha Roy, DebrupaLahiri, Mechanical, corrosion and biocompatibility behavior of Mg-3Zn-HA biodegradable composites for orthopaedic fixture accessories, *J MechBehav Biomed Mater.* 78 (2018) 442–454. <https://doi.org/10.1016/j.jmbbm.2017.11.030>
- [3] Z. Cui, W. Li, L. Cheng, D. Gong, W. Cheng, W. Wang, Effect of nano-HA content on the mechanical properties, degradation and biocompatible behavior of Mg-Zn/HA composite prepared by spark plasma sintering, *Mater Charact.* 151 (2019) 620–631. <https://doi.org/10.1016/j.matchar.2019.03.048>
- [4] E. Ghasali, M. Alizadeh, M. Niazmand, T. Ebadzadeh, Fabrication of magnesium-boron carbide metal matrix composite by powder metallurgy route: Comparison between microwave and spark plasma sintering, *J. Alloys Compd.* 697 (2017) 200-207. <https://doi.org/10.1016/j.jallcom.2016.12.146>
- [5] A. Shakil, S. Kumar Singh, B. Rajak, R.K. Gautam, U.S. Rao, In situ infiltration synthesis and characterization of magnesium metal matrix composite, *Mater. Today.* 21 (2) (2020) 1223-1228. <https://doi.org/10.1016/j.matpr.2020.01.073>.
- [6] I. Dinaharan, S.C. Vettivel, M. Balakrishnan, E.T. Akinlabi, Influence of processing route on microstructure and wear resistance of fly ash reinforced AZ31 magnesium matrix composites, *J. Alloys Compd.* 7 (2019) 155-165. <https://doi.org/10.1016/j.jma.2019.01.003>
- [7] A. Abbas, S. Huang, ECAP effects on microstructure and mechanical behavior of annealed WS<sub>2</sub>/AZ91 metal matrix composite, *J. Alloys Compd.* 835 (2020) 155466. <https://doi.org/10.1016/j.jallcom.2020.155466>
- [8] A. Maria, K. Anna, S. Igor, Evolution of the effective elastic properties of metal matrix composites during the synthesis, *Int. J. Eng. Sci.* 153 (2020) 103307. <https://doi.org/10.1016/j.ijengsci.2020.103307>
- [9] S. Jayasathyakawin, M. Ravichandran, N. Baskar, C. Anand Chairman, R. Balasundaram, Magnesium matrix composite for biomedical applications through powder metallurgy–Review, *Mater. Today.* 27 (2020) 736-741. <https://doi.org/10.1016/j.matpr.2019.12.003>

- [10] M. Rahman, Y. Li, C. Wen, HA coating on Mg alloys for biomedical applications: A review, *J. Mg Alloys*.8 (3) (2020) 929-943. <https://doi.org/10.1016/j.jma.2020.05.003>
- [11] S. Dinesh Kumar, M. Ravichandran, S. Sakthivelu, M. Meignanamoorthy, C. Chanakyan, S.V. Alagarsamy, Mechanical properties of magnesium-silicon carbide composite fabricated through powder metallurgy route, *Mater. Today*. 27 (2020) 1137-1141. <https://doi.org/10.1016/j.matpr.2020.01.592>
- [12] Huan Yu, Haiping Zhou, Yu Sun, Lili Ren, Zhipeng Wan, Lianxi Hu, Microstructures and mechanical properties of ultrafine-grained Ti/AZ31 magnesium matrix composite prepared by powder metallurgy, *Adv Powder Technol*. 29 (12) (2018) 3241-3249. <https://doi.org/10.1016/j.appt.2018.09.001>
- [13] N. Singh, U. Batra, Kamal Kumar, Anil Mahapatro, Investigating TiO<sub>2</sub>-HA-PCL hybrid coating as an efficient corrosion resistant barrier of ZM21 Mg alloy, *J. Mg Alloys*.9 (2) (2021) 627-646. <https://doi.org/10.1016/j.jma.2020.08.003>
- [14] S. Singh, C. Prakash, H. Singh, Deposition of HA-TiO<sub>2</sub> by plasma spray on  $\beta$ -phase Ti-35Nb-7Ta-5Zr alloy for hip stem: Characterization, mechanical properties, corrosion, and in-vitro bioactivity, *Surf Coat Technol*. 398 (2020) 126072. <https://doi.org/10.1016/j.surfcoat.2020.126072>
- [15] F. Munarin, P. Petrini, R. Gentilini, R.S. Pillai, S. Dire, M.C. Tanzi, V.M. Sglavo, Micro- and nano-hydroxyapatite as active reinforcement for soft biocomposites, *Int. J. Biol. Macromol*. 72 (2015) 199-209. <https://doi.org/10.1016/j.ijbiomac.2014.07.050>
- [16] C. Prakash, S. Singh, K. Verma, Sarabjeet S. Sidhu, S. Singh, Synthesis and characterization of Mg-Zn-Mn-HA composite by spark plasma sintering process for orthopedic applications, *Vacuum*. 155 (2018) 578-584. <https://doi.org/10.1016/j.vacuum.2018.06.063>
- [17] D. Liu, Y. Liu, Y. Zhao, Y. Huang, Minfang Chen, The hot deformation behavior and microstructure evolution of HA/Mg-3Zn-0.8Zr composites for biomedical application, *Mater SciEng C*. 77 (2017) 690-697. <https://doi.org/10.1016/j.msec.2017.03.239>
- [18] Q.C. Jiang, H.Y. Wang, B.X. Ma, Y. Wang, F. Zhao, Fabrication of B<sub>4</sub>C particulate reinforced magnesium matrix composite by powder metallurgy, *J. Alloy Compd*. 386 (1-2) (2005) 177-181. <https://doi.org/10.1016/j.jallcom.2004.06.015>
- [19] G. Xiong, Y. Nie, D. Ji, J. Li, C. Li, W. Li, Y. Zhu, H. Luo, Y. Wan, Characterization of biomedical hydroxyapatite/magnesium composites prepared by powder metallurgy

- assisted with microwave sintering, *Curr. Appl. Phys.* 16 (8) (2016) 830–836. <https://doi.org/10.1016/j.cap.2016.05.004>
- [20] F. Witte, N. Hort, C. Vogt, S. Cohen, Karl Ulrich Kainer, R. Willumeit, F. Feyerabend, Degradable biomaterials based on magnesium corrosion, *Curr Opin Solid State Mater Sci.* 12 (2008) 63–72. <https://doi.org/10.1016/j.cossms.2009.04.001>
- [21] L.F. Guleryuz, S. Ozan, D. Uzunsoy, R. Ipek, An investigation of the microstructure and mechanical properties of B<sub>4</sub>C reinforced PM magnesium matrix composites, *Powder Metall. Met. Ceram.* 51 (7-8) (2012) 456-462. <https://doi.org/10.1007/s11106-012-9455-9>.
- [22] H. Watanabe, T. Mukai, M. Mabuchi, K. Higashi, High-strain-rate superplasticity at low temperature in a ZK61 magnesium alloy produced by powder metallurgy, *Scripta Mater.* 41 (1999) 209-213. [https://doi.org/10.1016/S1359-6462\(99\)00155-4](https://doi.org/10.1016/S1359-6462(99)00155-4)
- [23] X. Gu, W. Zhou, Y. Zheng, L. Dong, Y. Xi, Donglang Chai, Microstructure, mechanical property, bio-corrosion and cytotoxicity evaluations of Mg/HA composites, *Mater SciEng C.* 30 (2010) 827–832. <https://doi.org/10.1016/j.msec.2010.03.016>
- [24] M. Carboneras, L.S. Hernandez, J.A. Del Valle, M.C. Garcia-Alonso, M.L. Escudero, Corrosion protection of different environmentally friendly coatings on powder metallurgy magnesium, *J. Alloys Compd.* 496 (1-2) (2010) 442-448. <https://doi.org/10.1016/j.jallcom.2010.02.043>
- [25] P. Bansal, G. Singh, H. Singh Sidhu, Investigation of surface properties and corrosion behavior of plasma sprayed HA/ZnO coatings prepared on AZ31 Mg alloy, *Surf Coat Technol.* 401 (2020) 126241. <https://doi.org/10.1016/j.surfcoat.2020.126241>
- [26] H. Watanabe, T. Mukai, M. Mabuchi, K. Higashi, Superplastic deformation mechanism in powder metallurgy magnesium alloys and composite, *Acta mater.* 49 (11) (2001) 2027-2037. [https://doi.org/10.1016/S1359-6454\(01\)00101-X](https://doi.org/10.1016/S1359-6454(01)00101-X)
- [27] T. Schubert, L. Ciupinski, W. Zielinski, A. Michalski, T. Weißgarber, B. Kieback, Interfacial characterization of Cu/diamond composites prepared by powder metallurgy for heat sink applications, *Scr. Mater.* 58 (2008) 263-266. <https://doi.org/10.1016/j.scriptamat.2007.10.011>
- [28] A.R. Khoei, A. RezaeiSameti, H. Mofatteh, Compaction simulation of crystalline nanopowders under cold compaction process with molecular dynamics analysis, *Powder Technol.* 373 (2020) 741-753. <https://doi.org/10.1016/j.powtec.2020.06.069>
- [29] M. Topuz, B. Dikici, M. Gavgali, M. Kaseem, Processing of Ti/(HA+ZrO<sub>2</sub>) biocomposite and 50% porous hybrid scaffolds with low Young's modulus by powder

- metallurgy: Comparing of structural, mechanical and corrosion properties, Mater. Today Commun. 29 (2021) 102813. <https://doi.org/10.1016/j.mtcomm.2021.102813>
- [30] F. Xie, J. Huang, S. Cao, X. He, Effects of hydroxyapatite addition on corrosion behavior and in-vitro bioactivity of Ti-10Mo matrix biocomposite, Mater. Today Commun. 31 (2022) 103787. <https://doi.org/10.1016/j.mtcomm.2022.103787>
- [31] E. Ghazizadeh, A.H. Jabbari, M. Sedighi, In vitro corrosion-fatigue behavior of biodegradable Mg/HA composite in simulated body fluid, J. Mg Alloys.9 (6) (2021) 2169-2184. <https://doi.org/10.1016/j.jma.2021.03.027>
- [32] M. Akmal, A. Raza, M. Mudasser Khan, M. Imran Khan, M. Asif Hussain, Effect of nano-hydroxyapatite reinforcement in mechanically alloyed NiTi composites for biomedical implant, Mater Sci Eng. 68 (2016) 30–36. <https://doi.org/10.1016/j.msec.2016.05.092>
- [33] C. Prakash, S. Singh, S. Ramakrishna, G. Krolczyk, Chi H. Le, Microwave sintering of porous Ti–Nb–HA composite with high strength and enhanced bioactivity for implant applications, J. Alloy Compd. 824 (2020) 153774. <https://doi.org/10.1016/j.jallcom.2020.153774>
- [34] X. Zhao, J. Zheng, W. Zhang, X. Chen, Z. Gui, Preparation of silicon coated-carbon fiber reinforced HA bio-ceramics for application of load-bearing bone, Ceram. Int. 46 (6) (2020) 7903-7911. <https://doi.org/10.1016/j.ceramint.2019.12.010>
- [35] Q. Gao, H. Liu, C. Cheng, K. Li, J. Zhang, C. Zhang, Y. Li, Preparation and Characterization of Activated Carbon from Wool Waste and the Comparison of Muffle Furnace and Microwave Heating Methods, Powder Technol. 249 (2013) 234-240. <https://doi.org/10.1016/j.powtec.2013.08.029>
- [36] K.S. Tun, M. Gupta, Improving mechanical properties of magnesium using nano-yttria reinforcement and microwave assisted powder metallurgy method, Compos Sci Technol. 67 (13) (2007) 2657–2664. <https://doi.org/10.1016/j.compscitech.2007.03.006>
- [37] B.P. Neville, A. Rabiei, Composite metal foams processed through powder metallurgy, Mater. Des. 29 (2008) 388-396. <https://doi.org/10.1016/j.matdes.2007.01.026>
- [38] G.K. Meenashisundaram, S. Seetharaman, M. Gupta, Enhancing overall tensile and compressive response of pure Mg using nano-TiB<sub>2</sub> particulates, Mater. Charact. 94 (2014) 178-188. <https://doi.org/10.1016/j.matchar.2014.05.021>
- [39] S.H. Roshan, H. EivazMohammadloo, A.A. Sarabi, M. Afshari, Biocompatible hybrid chitosan/hydroxyapatite coating applied on the AZ31 Mg alloy substrate: In-vitro

- corrosion, surface and structure studies, *Mater. Today Commun.* 30 (2022) 103153.  
<https://doi.org/10.1016/j.mtcomm.2022.103153>
- [40] N. Singh, U. Batra, K. Kumar, A. Mahapatro, Evaluation of corrosion resistance, mechanical integrity loss and biocompatibility of PCL/HA/TiO<sub>2</sub> hybrid coated biodegradable ZM21 Mg alloy, *J. Mg Alloys.* (2021) In Press, Corrected Proof.  
<https://doi.org/10.1016/j.jma.2021.10.004>
- [41] Ren-guo Guan, Aaron F. Cipriano, Zhan-yong Zhao, Jaclyn Lock, Di Tie, Tong Zhao, Tong Cui, Huinan Liu, Development and evaluation of a magnesium–zinc–strontium alloy for biomedical applications-Alloy processing, microstructure, mechanical properties, and biodegradation, *Mater. Sci. Eng C.* 33 (7) (2013) 3661-3669.  
<https://doi.org/10.1016/j.msec.2013.04.054>
- [42] B. Selvam, P. Marimuthu, R. Narayanasamy, V. Anandakrishnan, K.S. Tun, M. Gupta, M. Kamaraj, Dry sliding wear behavior of zinc oxide reinforced magnesium matrix nano-composites, *Mater. Des.* 58 (2014) 475-481.  
<https://doi.org/10.1016/j.matdes.2014.02.006>
- [43] S. Garcia-Rodríguez, B. Torres, A. Maroto, A.J. Lopez, E. Otero, J. Rams, Dry sliding wear behavior of globular AZ91 magnesium alloy and AZ91/ SiCp composites, *Wear.* 390-391 (2017) 1-10. <https://doi.org/10.1016/j.wear.2017.06.010>
- [44] C. Taltavull, A.J. Lopez, B. Torres, J. Rams, Dry sliding wear behaviour of laser surface melting treated AM60B magnesium alloy, *Surf. Coat. Technol.* 236 (2013) 368-379. <https://doi.org/10.1016/j.surfcoat.2013.10.015>
- [45] A.J. Lopez, P. Rodrigo, B. Torres, J. Rams, Dry sliding wear behavior of ZE41A magnesium alloy, *Wear.* 271 (11-12) (2011) 2836-2844.  
<https://doi.org/10.1016/j.wear.2011.05.043>
- [46] H.U. Yong, R.A.O. Li, Effect of particulate reinforcement on wear behavior of magnesium matrix composites, *Trans Nonferrous Met Soc China.* 22 (11) (2012) 2659–2664. [https://doi.org/10.1016/S1003-6326\(11\)61514-8](https://doi.org/10.1016/S1003-6326(11)61514-8)
- [47] H. Bolin, Y. Yingxia, X. Songsong, L. Zongmin, Effect of Ultrasonic Impact Treating on Wear Resistance and Microhardness of AZ91D Magnesium Alloy, *Rare Metal Mat Eng.* 46 (2017) 0017-0022. [https://doi.org/10.1016/S1875-5372\(17\)30070-X](https://doi.org/10.1016/S1875-5372(17)30070-X)
- [48] S. ZamaniKhalajabadi, N. Ahmad, S. Izman, A. Bin Haji Abu, W. Haider, M. Rafiq Abdul Kadir, In vitro biodegradation, electrochemical corrosion evaluations and

- mechanical properties of an Mg/HA/TiO<sub>2</sub> nanocomposite for biomedical applications, *J. Alloy Compd.* 696 (2017) 768-781. <https://doi.org/10.1016/j.jallcom.2016.11.106>
- [49] J.P. Davim, An experimental study of the tribological behaviour of the brass/steel pair, *J Mater Process Technol.* 100 (2000) 273–277. [https://doi.org/10.1016/S0924-0136\(99\)00491-4](https://doi.org/10.1016/S0924-0136(99)00491-4)
- [50] R.L. Deuis, C. Subramanian, J.M. Yellup, Abrasive wear of aluminium composites-a review, *Wear.* 201 (1-2) (1996) 132-144. [https://doi.org/10.1016/S0043-1648\(96\)07228-6](https://doi.org/10.1016/S0043-1648(96)07228-6)
- [51] H.R. Bakhsheshi-Rad, M.H. Idris, M.R. Abdul-Kadir, A. Ourdjini, M. Medraj, M. Daroonparvar, Mechanical and bio-corrosion properties of quaternary Mg–Ca–Mn–Zn alloys compared with binary Mg–Ca alloys, *Mater. Des.* 53 (2014) 283-292. <https://doi.org/10.1016/j.matdes.2013.06.055>
- [52] C.S. Ramesh, A.A. Khan, N. Ravikumar, P. Savanprabhu, Prediction of wear coefficient of Al6061–TiO<sub>2</sub> composites, *Wear.* 259 (2005) 602-608. <https://doi.org/10.1016/j.wear.2005.02.115>
- [53] C.S. Ramesh, R. Keshavamurthy, B.H. Channabasappa, S. Pramod, Friction and wear behavior of Ni–P coated Si<sub>3</sub>N<sub>4</sub> reinforced Al6061 composites, *Tribol Int.* 43 (3) (2010) 623-634. <https://doi.org/10.1016/j.triboint.2009.09.011>
- [54] K.W.H. Seah, M. Krishna, V.T. Vijayalakshmi, J. Uchil, Effects of temperature and reinforcement content on corrosion characteristics of LM13/albite composites, *Corros Sci.* 44 (2002) 761-772. [https://doi.org/10.1016/S0010-938X\(01\)00074-9](https://doi.org/10.1016/S0010-938X(01)00074-9)
- [55] K.S. Vinoth, R. Subramanian, S. Dharmalingam, B. Anandavel, Mechanical and tribological characteristics of stir-cast Al-Si10Mg and self-lubricating Al-Si10Mg/MOS<sub>2</sub> composites, *Mater Technol.* 46 (2012) 497-501.
- [56] R. Radha, D. Sreekanth, Insight of magnesium alloys and composites for orthopedic implant applications – a review, *J. Magnes. Alloy*, 5 (3) (2017) 286-312. <https://doi.org/10.1016/j.jma.2017.08.003>
- [57] D. Balaji, A. Arun premnath, A measurement of mechanical properties of AA - TiO<sub>2</sub> – Gr hybrid composite prepared through powder metallurgy process, *Measurement: Sensors*, 24 (2022) 100433. <https://doi.org/10.1016/j.measen.2022.100433>
- [58] A.M. Sankhla, K.M. Patel, Mayur A. Makhesana, K. Giasin, Danil Yu Pimenov, S. Wojciechowski, N. Khanna, Effect of mixing method and particle size on hardness and compressive strength of aluminium based metal matrix composite prepared through

- powder metallurgy route, *J. Mater. Res. Technol*, 18 (2022) 282-292. <https://doi.org/10.1016/j.jmrt.2022.02.094>
- [59] V.S.S. Venkatesh, Ashish B. Deoghare, Effect of microwave sintering on the mechanical characteristics of Al/kaoline/SiC hybrid composite fabricated through powder metallurgy techniques, *Mater. Chem. Phys*, 287 (2022) 126276. <https://doi.org/10.1016/j.matchemphys.2022.126276>
- [60] C.P. Samal, J.S. Parihar, D. Chaira, The effect of milling and sintering techniques on mechanical properties of Cu–graphite metal matrix composite prepared by powder metallurgy route, *J. Alloys Compd*, 569 (2013) 95-101. <https://doi.org/10.1016/j.jallcom.2013.03.122>
- [61] Qiang-Qiang Nie, Guo-Hong Chen, Bing Wang, Lei Yang, Wen-Ming Tang, Process optimization, microstructures and mechanical/thermal properties of Cu/Invar bi-metal matrix composites fabricated by spark plasma sintering, *Trans. Nonferrous Met. Soc. China*, 31 (10) (2021) 3050-3062. [https://doi.org/10.1016/S1003-6326\(21\)65714-X](https://doi.org/10.1016/S1003-6326(21)65714-X)
- [62] S. Dinesh Kumar, M. Ravichandran, A. Jeevika, B. Stalin, C. Kailasanathan, A. Karthick, Effect of ZrB<sub>2</sub> on microstructural, mechanical and corrosion behaviour of aluminium (AA7178) alloy matrix composite prepared by the stir casting route, *Ceram. Int*, 47 (9) (2021) 12951-12962. <https://doi.org/10.1016/j.ceramint.2021.01.158>
- [63] J.H. Zhang, K.B. Nie, K.K. Deng, J.G. Han, J.Y. Yi, Ultrahigh strength TiCnp /Mg–2Zn-0.8Sr-0.2Ca magnesium matrix composite processed by combining multidirectional forging with extrusion, *Compos. Commun*, 27 (2021) 100847. <https://doi.org/10.1016/j.coco.2021.100847>
- [64] J. Jiang, C. Collado, D. Keeley, B. Dodd, Room temperature formability of particle-reinforced metal matrix composites: forging, extrusion and deep drawing, *Compos*, 26 (11) (1995) 785-789. [https://doi.org/10.1016/0010-4361\(95\)98199-U](https://doi.org/10.1016/0010-4361(95)98199-U)
- [65] J. Zeng, Y. Yu, Z. Yan, H. Dai, H. Zhou, Preparation of the 0.4GNPs/Mg-8Al-1Sm magnesium matrix composites via plasma sintering and plasma forging two steps forming method, *Mater. Today Commun*, 34 (2023) 105345. <https://doi.org/10.1016/j.mtcomm.2023.105345>